The Meteoritical Society

Meteoritics & Planetary Science 59, Nr 11, 2956–2980 (2024)
doi: 10.1111/maps.14258

Fe, Zn, and Mg stable isotope systematics of acapulcoite lodranite clan meteorites

Stepan M. CHERNONOZHKIN[1,2]*, Lidia PITTARELLO[3], Genevieve HUBLET[4], Philippe CLAEYS[5], Vinciane DEBAILLE[4], Frank VANHAECKE[1], and Steven GODERIS[5]

[1]Atomic & Mass Spectrometry—A&MS Research Unit, Department of Chemistry, Ghent University, Ghent, Belgium
[2]Isotope Ratio Analysis Research Group, Chair of General and Analytical Chemistry, Montanuniversität Leoben, Leoben, Austria
[3]Naturhistorisches Museum Wien – NHMW, Vienna, Austria
[4]Laboratoire G-Time, Université Libre de Bruxelles, Brussels, Belgium
[5]Archaeology, Environmental Changes, and Geo-Chemistry (AMGC), Vrije Universiteit Brussel, Brussels, Belgium

***Correspondence**
Stepan M. Chernonozhkin, Atomic & Mass Spectrometry—A&MS Research Unit, Department of Chemistry, Ghent University, Campus Sterre, Krijgslaan, 281-S12, Ghent 9000, Belgium.
Email: stepan.chernonozhkin@gmail.com

(Received 15 November 2023; revision accepted 05 August 2024)

Abstract–The processes of planetary accretion and differentiation, whereby an unsorted mass of primitive solar system material evolves into a body composed of a silicate mantle and metallic core, remain poorly understood. Mass-dependent variations of the isotope ratios of non-traditional stable isotope systems in meteorites are known to record events in the nebula and planetary evolution processes. Partial melting and melt separation, evaporation and condensation, diffusion, and thermal equilibration between minerals at the parent body (PB) scale can be recorded in the isotopic signatures of meteorites. In this context, the acapulcoite–lodranite meteorite clan (ALC), which represents the products of thermal metamorphism and low-degree partial melting of a primitive asteroid, is an attractive target to study the processes of early planetary differentiation. Here, we present a comprehensive data set of mass-dependent Fe, Zn, and Mg isotope ratio variations in bulk ALC species, their separated silicate and metal phases, and in handpicked mineral fractions. These non-traditional stable isotope ratios are governed by mass-dependent isotope fractionation and provide a state-of-the-art perspective on the evolution of the ALC PB, which is complementary to interpretations based on the petrology, trace element composition, and isotope geochemistry of the ALC. None of the isotopic signatures of ALC species show convincing co-variation with the oxygen isotope ratios, which are considered to record nebular processes occurring prior to the PB formation. Iron isotopic compositions of ALC metal and silicate phases broadly fall on the isotherms within the temperature ranges predicted by pyroxene thermometry. The isotope ratios of Mg in ALC meteorites and their silicate minerals are within the range of chondritic meteorites, with only accessory spinel group minerals having significantly different compositions. Overall, the Mg and Fe isotopic signatures of the ALC species analyzed are in line with their formation as products of high-degree thermal metamorphism and low-degree partial melting of primitive precursors. The $\delta^{66/64}$Zn values of the ALC meteorites demonstrate a range of ~3.5‰ and the Zn is overall isotopically heavier than in chondrites. The superchondritic Zn isotopic signatures have possibly resulted from evaporative Zn losses, as observed for other meteorite parent bodies. This is unlikely to be the result of PB differentiation processes, as the Zn isotope ratio data show no covariation with the proxies of partial melting, such as the mass fractions of the platinum group and rare earth elements.

INTRODUCTION

Primitive achondrites (PA) form a group of meteorites which have grossly chondritic compositions and mineralogy, while at the same time displaying recrystallized igneous and/or metamorphic achondritic textures, reflecting low-degree partial melting of their chondritic precursors (Keil & McCoy, 2018; Krot et al., 2014). The acapulcoite lodranite meteorites clan (ALC, or acapodranites according to Krot et al., 2014) belongs to the PA. There are in total 194 meteorites of this family known according to the Meteoritical Bulletin database of September 2023 (91 of which are acapulcoites, 91 lodranites, 11 transitional acapulcoite/lodranites, and one anomalous lodranite Yamato 74357). ALC meteorites are fine- to medium-grained equigranular rocks with recrystallized textures, consisting of olivine, orthopyroxene, Ca-pyroxene, plagioclase, Fe-Ni metal, and some accessory minerals, such as chromite, phosphate, and sulfide (Keil & McCoy, 2018; Krot et al., 2014). Relict chondrules have been reported to occur in some acapulcoites. Lodranites are more coarse-grained than acapulcoites and contain less plagioclase, high-Ca pyroxene, and troilite. Lodranites reflect higher degrees of partial melting and higher equilibration temperatures (from ~5 to >10%, McCoy et al., 1997, and 1125–1250°C, Lucas et al., 2022) compared to acapulcoites (~1%–4% partial melting and 950–1100°C; Lucas et al., 2022; McCoy et al., 1997). The transitional acapulcoite/lodranites have intermediate textures and peak equilibration temperatures between those of acapulcoites and lodranites.

The elemental composition of ALC varies from chondritic to elemental signatures marked by extraction of plagioclase–clinopyroxene and metal–sulfide melts. The abundances and fractionation patterns of the highly siderophile elements suggest a continuum of metal–sulfide partial melting and melt extraction ranging from lower (acapulcoites) to higher (troilite-depleted lodranites) degrees, but also solid-melt re-distribution and accumulation in certain areas of the parent body (PB; i.e., pooling, Dhaliwal et al., 2017). The loss and migration of basaltic partial melts in ALC is reflected in their low Fe/Mg ratios relative to H chondrites, depleted alkali element abundances and fractionated patterns of rare earth elements (REE; Goodrich & Delaney, 2000; Keil & McCoy, 2018; Mittlefehldt, 2014; Morikawa & Nakamura, 1997). REE patterns of silicate minerals of ALC meteorites reflect a continuum of degrees of partial melting, both with and without melt migration, rather than a simple acapulcoite/lodranite bimodal classification (Floss, 2000).

The oxygen isotopic signatures of ALC meteorites fall into a characteristic array in the three-isotope space between the terrestrial fractionation line and the carbonaceous chondrite anhydrous minerals line, distinct from the characteristic fields of chondrites and other groups of PA. The ALC shows an average $\Delta^{17}O$ value of $-1.12 \pm 0.36‰$, with little to no systematic difference between acapulcoites and lodranites (Greenwood et al., 2017). The high level of heterogeneity within the clan and absence of a well-defined fractionation line are consistent with accretion from primordial components having different nebular sources, followed by incomplete PB melting and homogenization (Dhaliwal et al., 2017).

Nucleosynthetic isotopic anomalies (observed for, e.g., Ti, Cr, Zr, Mo) and depletions in the neutron-rich nuclides ^{50}Ti and ^{54}Cr link ALC to the asteroid Vesta sub-group meteorites, composed of HED, angrites, eucrites, mesosiderites, and brachinites, inferring an inner solar system origin (Render et al., 2022; Rüfenacht et al., 2023). The relationships between the ALC mineralogy and visual to infrared spectra suggest that the PB of ALC meteorites could sample a partially melted S-type asteroid located in the inner part of the asteroid belt (Lucas et al., 2019).

Overall, based on their texture, mineralogy, chemical composition, and O isotopic composition, the ALC clan is thought to originate from a single, partially melted PB ~520 km in diameter (Neumann et al., 2018), which initially had a composition similar to EL or H chondrites (Keil & McCoy, 2018), but differed from known chondrites in oxygen isotopic composition (Greenwood et al., 2017). The ALC's PB originated in the inner solar system (Render et al., 2022; Rüfenacht et al., 2023) ~1.5–2 Ma after the formation of calcium–aluminum-rich inclusions (CAI; Touboul et al., 2009). Heating by radiogenic decay of short-lived radionuclides caused low-degree partial melting, increasing from the outer layer to the center of the ALC parent asteroid, and melt migration, resulting in an "onion-shell" layered structure of the primordial PB. This is reflected in a continuum of metal-rich lodranites, lodranites, transitional acapulcoite–lodranites, acapulcoites, "primitive" acapulcoites with relict chondrules, and related metamorphosed precursor chondrites (e.g., GRV 020043; Li et al., 2018). The fractionation of the ALC was likely halted within the first ~5 Ma after CAIs formation by a catastrophic impact event and collisional fragmentation, followed by reassembly of the second-generation rubble-pile ALC PB, as recorded by the peak equilibration temperatures (Lucas et al., 2022). Only a short overview of ALC mineralogy, geochemistry, and petrogenesis is presented above, while the interested reader is referred to more detailed descriptions found in several reviews (Collinet & Grove, 2020; Keil & McCoy, 2018; Krot et al., 2014; Li et al., 2018; Lucas et al., 2022).

Early ceasing of the fractionation processes within the ALC PB, as evidenced by their ancient crystallization ages (e.g., Touboul et al., 2009), marks the group of ALC meteorites as a highly suited target to study how the

earliest stages of planetary differentiation in the solar system affected the isotope fractionation of non-traditional isotopic systems. Mass-dependent variation of the isotope ratios of novel "non-traditional" isotopic systems (e.g., Zn, Fe, Mg; Teng et al., 2017) in meteorites was successfully applied to study various differentiation processes in the early solar system. Isotope fractionation of Fe and Mg can record partial melting and extraction of metal and silicate melts (Dauphas et al., 2014; Schiller et al., 2017; Young & Scott, 2021), as well as the thermal histories of the equilibrated mineral assemblages (Dauphas et al., 2012; Huang et al., 2013). Isotope ratios of the moderately volatile element Zn are known to record evaporation processes in the early solar system (e.g., Dhaliwal et al., 2018; Paniello, Day, et al., 2012; Pringle et al., 2017). As such, the Fe, Mg, and Zn stable isotopic systems are highly suited to shed light onto the processes of early differentiation and volatile loss of the ALC's PB.

The overall goal of this work was to study the Fe, Mg, and Zn stable isotope geochemistry of ALC meteorites at the bulk scale and mineral level, as it can provide a perspective that is complementary to the known elemental and isotope geochemistry, petrology, and thermochemistry. In particular, the goal was to assess the role of early thermal metamorphism, evaporation, and the mobility of metal and silicate melts in the evolution of the isotopic signatures, as these processes shed light onto the first critical stages of the planetary evolution in the solar system. An additional aim of this work was to evaluate whether the signatures of the non-traditional stable isotopic systems are inherited from the early non-homogenous Solar Nebula stage.

MATERIALS AND METHODS

Samples and Reference Materials

Reference materials of mafic and ultramafic rock powders BHVO-2, BCR-1, BCR-2 (United States Geological Survey, Denver, CO, USA), JP-1, and JB-1b (Geological Survey of Japan, Tsukuba, Japan) were processed together with the meteorite samples and used for quality assurance and quality control of the isotope ratio data. Certified isotopic reference materials and reference materials for which the isotopic composition was characterized previously for Mg (DSM3 by Galy et al., 2003 and ERM-AE143, Federal Institute for Materials Research and Testing BAM, Berlin, Germany), Fe (IRMM-014 and IRMM-524a, Institute for Reference Materials and Measurements IRMM, Geel, Belgium), and Zn (IRMM-3702 and the Johnson Mattey 3-0749L Zn solution, also known as JMC-Lyon and characterized by Maréchal et al., 1999) were used throughout this work for correction of the bias introduced by instrumental isotope fractionation. Single-element stock solutions of Fe, Mg, and Zn (Inorganic Ventures, USA) with previously characterized isotopic composition were used as in-house isotopic standards (Fe-A&MS lot D2-FE03110, Mg-A&MS lot K2-MG650434 and Zn-A&MS lot D2-ZN02061, González de Vega et al., 2020) for quality assurance/quality control.

In total, two acapulcoites, two lodranites, and one meteorite classified as transitional acapulcoite–lodranite were provided by the Department of Mineral Sciences of the Smithsonian Institution and Astromaterials Curation Office at NASA Johnson Space Center (NASA-JSC, Houston, TX, USA) from the NASA Antarctic meteorite collection recovered by the Antarctic Search for Meteorites (ANSMET) program. Two acapulcoites were lent for this study by the National History Museum London from the collection of historic meteorites and meteorites collected from hot deserts. For each meteorite, both chips and polished sections (either thin sections or epoxy mounts) were made available. The chips were used for solution analysis of bulk samples, fractions, and mineral separates after acid digestion, while the polished sections were used for in situ and spatially resolved analysis. A full list of the ALC meteorites studied in this work is shown in Table 1.

In Situ Characterization

The polished sections of the meteorites were characterized preliminarily using in situ analytical techniques: scanning electron microscopy (SEM), micro-X ray fluorescence spectrometry (μXRF), electron microprobe analysis (EMPA), and laser ablation ICP-mass spectrometry (LA-ICP-MS). A full description of the analytical procedures for these in situ analyses can be found in (Chernonozhkin, Goderis, et al. 2021; Chernonozhkin, McKibbin, et al. 2021; Soens et al., 2021). In brief, a Bruker M4 Tornado XRF instrument in operation at the AMGC-VUB (Brussels, Belgium) was used to obtain 2-D element distribution maps of the polished sections of the meteorites studied. A JEOL JSMIT-300 SEM unit, coupled to an Oxford energy-dispersive spectrometer (EDS) in operation at VUB was used for producing backscattered electrons (BSE) maps of the entire 1-inch polished sections of the meteorites and for preliminary mineral identification. The μXRF and SEM-BSE maps were further used to identify suitable locations for LA-ICP-MS trace element analysis of selected minerals of the meteorites.

The LA-ICP-MS analysis was carried out at A&MS-UGent (Ghent, Belgium) by coupling a Teledyne Cetac Analyte G2 LA-system to an Agilent Technologies 8800 tandem ICP-MS instrument (Chernonozhkin, Goderis, et al. 2021; Chernonozhkin, McKibbin, et al. 2021). Field-

TABLE 1. List of ALC meteorites studied in this work, their classification, reference mineral, oxygen isotopic composition, and reported Ir/Pd ratio. The mineral composition and weathering degree from the Meteoritical Bulletin Database of 2021.

	Group	Fall/find	Weathering	Origin, institution	Olivine	Pyroxene	$\delta^{17}O$, ‰ ± SD	$\delta^{18}O$, ‰ ± SD	$\Delta^{17}O$, ‰	Ir/Pd	Ref.
ALHA 81187	ACA	Find	B/C	NASA-JSC	Fo_{96}	$Wo_{3.2}Fs_{6.5}$; $Wo_{42.5}Fs_{3.2}$	−0.14 ± 0.06	1.94 ± 0.16	−1.16	1.49	[a,b,c]
MET 01212	ACA	Find	B/C	NASA-JSC	$Fo_{91\text{-}92}$	$En_{92}Fs_{8}$ $Wo_{44\text{-}46}Fs_{3\text{-}4}$					
Dhofar 125	ACA[d]	Find	W1/2	NHM-L	$Fo_{91.5}$	$Wo_{1.9}Fs_{7.7}$; $Wo_{43.8}Fs_{3.7}$	0.92	3.97	−1.16		[a,b]
Monument Draw	ACA	Find	—	NHM-L	$Fo_{89.9}$	$Wo_{1.7}Fs_{10.6}$	1.04 ± 0.04	3.78 ± 0.06	−0.94		[a]
EET 84302	ACA/LOD[e]	Find	B/C	NASA-JSC	Fo_{92}	$Wo_{2.5}Fs_{8.2}$; $Wo_{43.7}Fs_{5.6}$	0.21 ± 0.05	2.73 ± 0.10	−1.22	1.88	[a,b,c]
GRA 95209	LOD	Find	B	NASA-JSC	$Fo_{92.7}$	$Wo_{3.2}Fs_{7.2}$; $Wo_{42.9}Fs_{3.7}$	−0.86 ± 0.15	1.03 ± 0.31	−1.39	1.90	[a,b,c]
LAR 06605	LOD[e]	Find	B	NASA-JSC	Fo_{88}	Fs_{12}					[a,b]

Abbreviations: ACA, acapulcoite; ACA/LOD, transitional acapulcoite/lodranite member; LOD, lodranite.

[a]Greenwood et al. (2017).

[b]Keil and McCoy (2018).

[c]Dhaliwal et al. (2017).

[d]A relict chondrule has been found in the thick section of Dhofar 125, which assigns it to the "primitive" acapulcoite group in the spectrum of acapulcoite lodranite clan meteorites (see Figure S1 in the ESI for μXRF images).

[e]Different sources classify this specimen as either lodranite or transitional acapulcoite/lodranite clan member. NASA-JSC—allocated by the NASA meteorite working group at the Smithsonian Institution and Astromaterials Curation Office at NASA Johnson Space Center; NHM-L—National History Museum London.

emission EMPA analysis was performed on two of the ALC meteorites (EET 84302 and LAR 06605) using a JEOL JXA 8530-F unit equipped with five wavelength-dispersive spectrometers (WDS) at the Natural History Museum of Vienna (Austria), with 20 nA probe current, using natural and synthetic reference materials for calibration and applying ZAF corrections. Detection limits for the silicate and chromite calibration are 150 $\mu g\,g^{-1}$ for SiO_2, 160 $\mu g\,g^{-1}$ for TiO_2, 230 $\mu g\,g^{-1}$ for V_2O_3, 100 $\mu g\,g^{-1}$ for Al_2O_3, 510 $\mu g\,g^{-1}$ for Cr_2O_3, 110 $\mu g\,g^{-1}$ for MgO, 100 $\mu g\,g^{-1}$ for CaO, 320 $\mu g\,g^{-1}$ for MnO, 300 $\mu g\,g^{-1}$ for FeO, 440 $\mu g\,g^{-1}$ for NiO, and 120 $\mu g\,g^{-1}$ for Na_2O, whereas for the metal calibration these are 120 $\mu g\,g^{-1}$ for P, 70 $\mu g\,g^{-1}$ for S, 330 $\mu g\,g^{-1}$ for Mn, 390 $\mu g\,g^{-1}$ for Fe, 300 $\mu g\,g^{-1}$ for Co, and 300 $\mu g\,g^{-1}$ for Ni.

Meteorite Sample Preparation and Mineral Separation

The meteorite sample preparation for MC-ICP-MS isotopic analysis was carried out in the dedicated laboratories of the Laboratoire G-Time, Université libre de Bruxelles (ULB). One to two grams of the meteorite chips were ground in a pre-cleaned agate mortar. The "whole rock" fractions were produced by fine grinding of ~200 mg of the initial chips. The rest was ground gently and separated into the size fractions <150 and 150–250 μm with a stack of corresponding sieves. All size fractions were then iteratively separated using an Nd hand magnet (3–5 times) into their magnetic and non-magnetic parts.

The "metal" fractions were prepared by dissolving the magnetic fractions selected by hand magnet in 6 M HCl, followed by filtering off the remaining undigested silicate. As such, the metal fractions represent a mixture of kamacite and taenite Fe-Ni metal, with some contribution of sulfide, although in the acapulcoites and especially in lodranites, little to no troilite is observed based on μXRF and SEM analysis of the polished sections. The 50–100 mg of the non-magnetic portions of the <150 μm size fractions produced by iterative Nd hand magnet separation were analyzed as "silicate".

The non-magnetic fractions produced by hand magnet separation of the 150- to 250-μm meteorite fractions were further processed using a Frantz isodynamic magnetic separator, which allowed magnetic and non-magnetic fractions to be collected. The Frantz processing of the non-magnetic phases was repeated multiple times at increasing current, with an increment of 0.1 A, until the absence of opaque metal phases in the non-magnetic fractions was confirmed using an optical binocular microscope. As complete separation of olivine and pyroxene minerals of ALC based on magnetic susceptibility is complicated because of the compositions of the minerals, the mineral fractions obtained by Frantz isodynamic magnetic separation were further purified by handpicking under a binocular microscope to produce 0.5–10 mg of "olivine" and "pyroxene" separates at the mineral laboratories of ULB and VUB (Brussels, Belgium). The use of heavy liquids for mineral separation was avoided to prevent contamination and/or mobilization of Zn. Due to the very small amount of material available for handpicking, it was frequently not possible to characterize the single mineral separates using SEM-EDS, and as such the "pyroxene" fractions used for isotopic analysis should be considered mixtures of pyroxenes of different compositions.

In addition to the handpicked "olivine" and "pyroxene," fractions of dark opaque minerals, identified as "chromite," were handpicked from the acapulcoites MET 01212, EET 84302, and lodranite LAR 06605. As it was not possible to confirm the "chromite" fractions by SEM-EDS due to their extremely small mass (<1 mg), they are identified here as chromite based on a combination of their non-magnetic dark opaque mineralogy, appearance, and refractory nature. These fractions did not digest during high-pressure microwave-assisted acid digestion conditions sufficient to dissolve any silicate phase. The complete digestion of these phases required repeated microwave acid digestion runs at higher temperature and pressure (300°C and 199 bar).

MC-ICP-MS High Precision Fe, Mg, and Zn Isotopic Analysis

Delta values for Fe, Mg, and Zn were measured in the meteorite "whole rock," "metal," "silicate," and single mineral fractions, and in geological reference materials (GRMs) following the protocols described earlier, so for details on reagents and labware used for sample preparation, the reader is referred to these earlier publications (Chernonozhkin et al., 2016; González de Vega et al., 2020; Grigoryan et al., 2020; Van Heghe et al., 2012).

Briefly, the sample and GRM powders were digested at A&MS UGent utilizing a two-step microwave-assisted digestion procedure using a high-pressure Multiwave 7000 unit (Anton Paar, Graz, Austria). Metal fractions of meteorites were digested in Savillex™ Teflon beakers using 6 M HCl. Iron and Zn isolation from the sample matrices was performed using an ion exchange chromatographic procedure carried out in trace metal class-10 clean laboratories (PicoTrace, Germany) at A&MS-UGent, relying on the use of AG MP-1M strong anion exchange resin in HCl media. The isolation procedure was initially described by Maréchal et al. (1999), and the column calibration is from Van Heghe et al. (2012). Magnesium was isolated from the sample matrix using AG50W-X8 strong cation exchanger in HCl/HF/acetone media (Wombacher et al., 2009), and

the column calibration reported in González de Vega et al. (2020) was relied on.

The high-precision isotope ratio measurements of Fe, Mg, and Zn solutions were carried out at A&MS-UGent using a Thermo Scientific Neptune *Plus* multi-collector ICP-MS unit operated in pseudo medium mass resolution on the interference-free shoulder of the spectral peaks of interest, while aspirating sample solution via a 100 µL min^{-1} PFA concentric nebulizer mounted onto a dual spray chamber (with a cyclonic and a Scott-type sub-unit). For further details about the instrument settings, the reader is referred to Chernonozhkin et al. (2016); González de Vega et al. (2020); Grigoryan et al. (2020); Van Heghe et al. (2012). The instrumental isotope fractionation of Fe and Zn was corrected for using a regression mathematic correction relying on the model of Baxter et al. (2006; using Ni and Cu isotope ratios as internal calibrators for Fe and Zn, respectively), followed by a sample standard bracketing (SSB) external correction. The instrumental isotope fractionation correction relied solely on SSB external correction for Mg. The isotope ratio data are reported in permil (‰) using the delta notation, calculated according to Equations 1–3, relative to IRMM-014, DSM3, and JMC-Lyon for Fe, Mg, and Zn, respectively.

$$\delta^{x/54}\mathrm{Fe} = \left(\frac{\left({}^{x}\mathrm{Fe}/{}^{54}\mathrm{Fe}\right)_{\mathrm{sample}}}{\left({}^{x}\mathrm{Fe}/{}^{54}\mathrm{Fe}\right)_{\mathrm{IRMM-014}}} - 1 \right) \times 1000 \quad (1)$$

$$\delta^{y/24}\mathrm{Mg} = \left(\frac{\left({}^{y}\mathrm{Mg}/{}^{24}\mathrm{Mg}\right)_{\mathrm{sample}}}{\left({}^{y}\mathrm{Mg}/{}^{24}\mathrm{Mg}\right)_{\mathrm{DSM3}}} - 1 \right) \times 1000 \quad (2)$$

$$\delta^{z/64}\mathrm{Zn} = \left(\frac{\left({}^{z}\mathrm{Zn}/{}^{64}\mathrm{Zn}\right)_{\mathrm{sample}}}{\left({}^{z}\mathrm{Zn}/{}^{64}\mathrm{Zn}\right)_{\mathrm{JMC-Lyon}}} - 1 \right) \times 1000 \quad (3)$$

Here, x stands for 56 or 57 for the isotopes of Fe, y stands for 25 or 26 for the isotopes of Mg and z stands for 66, 67, or 68 for the isotopes of Zn. A detailed list of all analyses carried out for each meteorite in this work is provided in Table 2. Several GRMs and blanks were run with each batch of isolations for QA/QC. The repeatability and reproducibility of the isotopic data are discussed in González de Vega et al. (2020), in which the results of GRM measurements within a period of several years are presented. On average, the expanded uncertainty (U) of the $\delta^{56/54}$Fe and $\delta^{26/24}$Mg values obtained in the laboratory over a period of several years was 0.050‰ and 0.082‰ (González de Vega et al., 2020). The measurement uncertainty of the isotope ratio data is provided as 2SD of multiple measurements of the sample solution within a period of several days, analyzed in multiple analytical sessions, and as such represents intermediate precision. The intermediate precision presented in such way tends to be higher than the repeatability.

RESULTS

The polished sections of the ALC examined with the optical microscope exhibit typical characteristics for this meteorite clan. However, it should be noted that the following petrographic descriptions are based on observations limited to a small portion (1-inch round sections) of generally heterogeneous materials, whereas the chemical analyses based on separates and bulk

TABLE 2. List of analyses carried out on each meteorite studied in this work.

				MC-ICP-MS		
	Group	EMPA	LA-ICP-MS	Mg	Fe	Zn
ALHA 81187	ACA	—[a]	LA-ICP-MS	Bulk, slc, ol, px	Bulk, slc, met, ol, px	Bulk, slc, met, ol, px
MET 01212	ACA	—	LA-ICP-MS	Bulk, slc, ol, px, chr	Bulk, slc, met, ol, px, chr	Bulk, slc, met, ol, px, chr
Dhofar 125	ACA	—	—[b]	Bulk, slc	Bulk, slc, met	Bulk, slc, met
Monument Draw	ACA	—	LA-ICP-MS	Bulk	Bulk	Bulk
EET 84302	ACA/ LOD	EMPA	LA-ICP-MS	Bulk, slc, ol, px, chr	Bulk, slc, met, ol, chr	Bulk, slc, ol, px, chr
GRA 95209	LOD	—	LA-ICP-MS	Bulk	Bulk	Bulk
LAR 06605	LOD	EMPA	LA-ICP-MS	Bulk, slc, ol, px, chr	Bulk, met, slc, ol, px, chr	Bulk, slc, ol, px, chr

[a]Polished sections of some meteorites were not analyzed by EMPA due to the restrictions in instrument time.
[b]Mineral grain size is too small for robust mineral identification and LA-ICP-MS analysis with 80-µm spot size; bulk, slc, met—isotope ratio measurements of Fe, Mg, and Zn in the digested powders of whole rock, fractions that are not-magnetic with respect to the hand magnet, and fractions that are magnetic with respect to the hand magnet, respectively. Ol, px, chr—handpicked mineral separates of olivine, pyroxene (of unidentified composition), and chromite, respectively.

meteorites were performed on other sample chips. The samples mainly consist of pyroxene, olivine, plagioclase, and opaque minerals, mostly Fe-Ni metal, phosphide, and sulfides. The acapulcoite members exhibit fine- to medium-grained equigranular textures, with olivine being less abundant than pyroxene. A single relic chondrule has been observed in the Dhofar 125 acapulcoite. The polished thin (approximately 30 μm) section of the MET 01212 acapulcoite exhibits a heterogeneous distribution of metal grains throughout the sample, with one domain characterized by a coarse-grained metal population (average grain size of 500 μm) with the other exhibiting fine-grained metal and silicate. The polished thin section of GRA 95209 lodranite (note that GRA 95209 is considered transitional acapulcoite/lodranite in Dhaliwal et al., 2017) displays a medium to coarse grain size, but also in this sample two domains can be distinguished based on their grain size and mineralogy: one domain is fine-grained, contains plagioclase (up to 500 μm) and a small amount of metal, the other is dominated by coarse-grained metal (up to 2 mm in size) and a lack of plagioclase and sulfides. The transition between the two domains is gradational. In addition, this sample is crosscut by thin metal veins, locally injected along grain boundaries between silicates. This may be suggestive of a transitional classification for GRA 95209. The LAR 06605 lodranite and the intermediate acapulcoite/lodranite EET 84302 exhibit equigranular coarse-grained assemblages, and both are relatively poor in plagioclase and contain large metal clusters (up to several mm in size). The polished section from EET 84302, examined in detail using electron microscopy during EMPA sessions, has a coarse-grained granular texture. The subrounded silicate minerals with an average size of approximately 100 μm are surrounded by a thin film of metal, connecting larger metal grains (several hundreds of micrometers). Chromite occurs as small (approximately 30 μm in diameter) rounded grains within olivine. Locally, pyroxene shows fine-grained exsolutions. When examined using electron microscopy, LAR 06605 showed a similar appearance but is on average coarser-grained and the metal portions appear less weathered than in the fragment of EET 84302 (Figure S7).

The composition of olivine in the ALC samples is $Fa_{4\text{-}12}$, of which the two pyroxenes are $Wo_{41\text{-}46}$ and $Fs_{6.4\text{–}12}$ (Keil & McCoy, 2018; Lucas et al., 2019). The major element compositions of the mineral cores of EET 84302 and LAR 06605 as measured by EMPA are shown in Table 3, and are $Fa_{8\text{-}10}$ for olivine, and $Wo_{2\text{-}3}Fs_{9\text{-}12}$ and $Wo_{43\text{-}46}Fs_4$ for the two pyroxenes. These results are in good to excellent agreement with the literature values (e.g., Keil & McCoy, 2018; Lucas et al., 2019). In previous work, Lucas et al. (2022) determined the two-pyroxene last equilibration temperature to be in the range of 948–1114°C for Dhofar 125, MET 01212, ALH 81187, EET 84302, GRA 95209, and LAR 06605. The last equilibration temperatures, calculated in this work for two meteorites using the thermometers and the calibrations of Putirka (2008) and Nakamuta et al. (2017), assuming that the phases were in equilibrium before the melting, are summarized in Table 3. The equilibration temperature of EET 84302 is in excellent agreement with that reported earlier (1021°C; Lucas et al., 2022), while that of LAR 06605 is somewhat lower than that measured in previous work (980–983 vs. 1047°C; Lucas et al., 2022), but still within the range of other ALC meteorites.

The mass fractions of trace and minor elements in the mineral cores of ALC meteorites are presented in Table 4, and are in good agreement with those reported by Lucas et al. (2022), especially for high-Ca pyroxene. The LA-ICP-MS results for olivine and low-Ca pyroxene, which tend to be extremely depleted in light REE, tend to deviate from published earlier data (Floss, 2000), likely as a result of terrestrial weathering and contamination.

The results for the isotope ratios of Fe, Mg, and Zn (expressed as delta values) of the GRMs are in good agreement with those reported earlier (e.g., compiled values in GeoRem database; Jochum et al., 2005). On average, the intermediate precision (equivalent to formerly known long-term precision) presented as 2SD of multiple measurements of the sample solution in a period of few days, is 0.093‰, 0.053‰, and 0.18‰ for $\delta^{56/54}$Fe, $\delta^{26/24}$Mg, and $\delta^{66/64}$Zn, respectively. The isotopic compositions of Fe, Mg, and Zn in the whole rock fractions of ALC meteorites, their silicate and metal separates, the handpicked mineral fractions, and in the GRMs are shown in Figure 1 and in Table 5. GRM $\delta^{56/54}$Fe range from −0.013 to +0.19‰, $\delta^{26/24}$Mg from −0.359‰ to −0.182‰, and $\delta^{66/64}$Zn from −0.056‰ to 2.18‰. The Fe, Mg, and Zn isotope ratios testify of mass-dependent isotope fractionation and fall onto the terrestrial fractionation lines within their associated uncertainties (Figure S8). When plotting $\delta^{26/24}$Mg versus $\delta^{25/24}$Mg, the regression line goes through the origin (intercept of 0.0017 ± 0.0134) and has a slope (0.512 ± 0.071) identical to that of the terrestrial fractionation line within measurement uncertainty (Figure S8). At the level of measurement uncertainty attained in this work, no radiogenic ^{26}Mg ingrowth from the decay of ^{26}Al has been observed. Measurement protocols with higher precision, capable of resolving extremely small variations of ^{26}Mg of radiogenic origin (e.g., Larsen et al., 2016), are not practical for Mg stable isotope analysis. The Mg isotopic signatures measured in bulk ALC meteorites in this work are in agreement with the only $\delta^{26/24}$Mg data available in the literature ($\delta^{26/24}\text{Mg} = -0.236 \pm 0.045$ for the Acapulco meteorite, Sedaghatpour & Teng, 2016).

The mean $\delta^{56/54}$Fe measurement results for whole rock ALC ($\delta^{56/54}\text{Fe} = 0.080 \pm 0.081$‰, SD, $n = 7$) are higher

TABLE 3. Results of EMPA measurements of the mafic mineral cores of two ALC meteorites, and the results of pyroxene geothermometer application.

	Mineral	Fa#	Wo	En	Fs	FeO (wt%)	MgO (wt%)	Cr_2O_3 (wt%)	MnO (wt%)	CaO (wt%)	Na_2O (wt%)	Al_2O_3 (wt%)	T (°C)
EET 84302	oliv	8.0				8.07 ± 0.14	52.13 ± 0.88	0.02 ± 0.05	0.44 ± 0.10	0.04 ± 0.01	bdl	bdl	1032/955[a]
ACA/LOD	cpx		43	53	4	2.21 ± 0.20	19.07 ± 0.67	1.47 ± 0.05	0.37 ± 0.04	21.89 ± 0.9	0.716 ± 0.014	1.06 ± 0.05	1036[b]
	opx		2	89	9	5.51 ± 0.08	35.42 ± 0.60	0.41 ± 0.05	0.51 ± 0.04	1.15 ± 0.08	0.026 ± 0.016	0.45 ± 0.06	
LAR 06605	oliv	10.6				10.71 ± 0.59	50.24 ± 0.71	0.04 ± 0.03	0.48 ± 0.05	0.12 ± 0.01	bdl	bdl	836/1107[a]
LOD	cpx		46	50	4	2.55 ± 0.23	18.07 ± 0.05	1.60 ± 0.19	0.26 ± 0.26	23.05 ± 0.25	0.906 ± 0.026	0.60 ± 0.02	983[b]
	opx		3	86	11	7.54 ± 0.13	33.87 ± 0.65	0.43 ± 0.12	0.54 ± 0.03	1.59 ± 0.54	0.044 ± 0.028	0.34 ± 0.07	

Abbreviation: bdl, below detection limit.

[a]Equilibration temperature calculated using the geothermometer with the calibration of Nakamuta et al. (2017) for cpx and opx, respectively.

[b]Equilibration temperature calculated using the geothermometer with the calibration of Putirka (2008) at 2.8 kbar (LAR 06605) and 3.6 kbar (EET 84302). Average compositions for EET 84302 are based on the analysis of three opx, five cpx, and three ol grains. Average compositions for LAR 06605 are based on the analysis of six opx, three cpx, and seven ol grains.

TABLE 4. Results of LA-ICP-MS analysis of the silicate mineral cores in ALC meteorites.

	Li	P	Sc	Ti	V	Cr	Mn	Co	Ni	Cu	Zn	Sr	Y	Zr	Cd	Sn	Sb	Cs	Ba	Hf	Pb	Th	U
Detection limits[a]	0.008	0.4	0.008	0.2	0.02	0.09	0.05	0.01	0.09	0.05	0.07	0.01	0.005	0.02	0.02	0.03	0.004	0.002	0.05	0.003	0.006	0.004	0.001
ALHA81187 (*ACA*)																							
ol	—	—	—	150	—	2300	3700	360	3900	5.5	110	34	—	6.8	—	—	0.25	—	10	0.24	0.47	0.040	0.085	
pig	—	—	—	180	—	5800	4300	34	480	7.9	230	34	—	—	—	—	—	—	—	0.082	0.42	0.157	0.11	
aug	—	—	—	2000	—	11,000	2700	38	460	3.2	65	38	16	4.9	—	0.16	—	—	10	0.51	0.45	0.041	0.008	
MET 01212 (*ACA*)																							
ol	—	—	—	340	—	1700	4000	30	390	7.1	190	35	—	—	3.6	1.6	—	—	11	—	0.70	0.022	—	
pig	—	—	—	150	—	630	1900	5.0	85	3.8	57	50	3.3	97	—	40	0.14	0.22	76	2.4	4.1	1.35	0.63	
aug	—	—	—	2500	—	9500	1600	30	270	8.5	34	43	16	70	50	8.6	0.24	0.20	28	2.0	1.5	0.538	0.15	
chr	—	—	—	7100	—	—	9100	11	4.6	1.4	6700	—	—	—	—	0.38	—	—	10	—	0.44	—	—	
Monument Draw (*ACA*)																							
ol	—	—	—	280	—	1700	4300	64	850	14	98	40	—	—	0.23	0.41	—	—	54	0.018	1.1	0.178	0.86	
pig	—	—	—	—	—	370	3900	18	230	2.8	160	89	—	—	—	0.12	—	—	12	0.10	0.41	0.279	0.17	
aug	—	—	—	1600	—	6400	2300	41	780	8.5	27	38	12	56	—	0.11	—	—	11	1.7	0.50	0.030	0.82	
EET 84302 (*ACA*/*LOD transitional*)																							
ol1	4.0	57	1.7	—	26	370	4100	6.8	37	21	190	140	—		—	—	—	—	—	—	—	—	0.084
ol2	3.6	61	1.2	—	23	770	3700	4.6	19	0.12	170	88	—	—	—	3.8	—	—	—	—	—	—	—
pig1	1.1	—	10	500	100	3400	4200	3.2	7.1	1.2	190	42	0.83	0.13	—	—	—	—	14	—	—	—	0.13
pig2	0.96	17	11	530	97	3000	4200	6.3	54	42	170	42	0.57	0.15	—	—	—	—	14	—	—	—	—
aug1	1.6	11	56	1800	370	10,000	2500	6.3	84	—	55	46	20	33	—	25	—	—	14	1.0	0.34	0.125	0.007
aug2	1.9	13	64	2100	420	11,000	2600	2.3	12	4.6	54	48	26	45	—	—	—	—	14	1.6	0.40	0.158	0.010
GRA 95209 (*LOD*)																							
ol	—	—	—	—	—	5500	3400	23	35	1.8	480	250	—	—	—	0.11	0.085	—	6.8	—	—	—	0.23	
pig	—	—	—	520	—	4000	3900	200	2800	1.8	11	45	—	—	—	110	—	—	14	—	0.75	0.089	—	
aug	—	—	—	2200	—	11,000	2900	44	730	2.2	46	38	19	20	—	—	—	0.18	5.1	0.92	0.78	0.030	0.16	
plag	0.90	—	9.2	340	81	2900	4000	11	120	79	150	43	0.40	0.050	—	—	—	—	—	—	—	—	—	
LAR 06605 (*LOD*)																							
ol1	2.8	92	2.0	—	15	120	4000	4.7	15	11	210	—	—	—	—	6.6	—	—	—	—	0.68	—	0.10	
ol2	3.4	120	1.8	—	17	92	4000	4.1	14	5.5	270	—	—	1.9	—	9.4	—	—	—	—	—	—	—	
pig1	0.47	10	13	430	110	4000	4500	4.9	10	—	270	—	0.71	0.49	0.51	7.6	—	5.4	9.1	—	—	—	—	
pig2	0.63	7.0	12	390	110	4400	4400	4.7	7.5	4.7	260	42	0.93	0.62	0.43	13	13		—	—	0.33	—	—	
aug	0.43	20	50	1000	340	11,000	2700	6.2	66	4.0	82	50	12	1.6	—	7.5	6.7	—	—	0.008	0.35	—	—	

TABLE 4. *Continued.* Results of LA-ICP-MS analysis of the silicate mineral cores in ALC meteorites.

	La	Ce	Pr	Nd	Sm	Eu	Gd	Tb	Dy	Ho	Er	Tm	Yb	Lu
Detection limits[a]	0.007	0.009	0.003	0.012	0.006	0.002	0.009	0.001	0.004	0.001	0.002	0.001	0.003	0.001
ALHA 81187 (*ACA*)														
ol	0.25	0.90	0.20	1.1	0.24	0.13	0.28	0.058	0.36	0.056	0.15	0.024	0.12	0.030
pig	0.23	0.88	0.20	1.1	0.23	0.11	0.24	0.054	0.33	0.043	0.19	0.031	0.24	0.047
aug	1.4	6.6	1.3	7.1	2.4	0.18	3.1	0.54	3.6	0.68	1.8	0.25	1.4	0.22
MET 01212 (*ACA*)														
ol	3.5	3.9	0.17	0.90	0.64	0.11	0.11	0.019	0.10	—	0.039	0.003	0.080	0.019
pig	4.0	7.1	1.0	3.6	0.64	0.21	0.58	0.084	0.43	0.071	0.29	0.048	0.35	0.066
aug	2.9	8.8	1.5	7.3	2.3	0.18	2.8	0.51	3.1	0.63	1.8	0.24	1.4	0.21
chr	—	—	0.17	0.92	—	0.11	0.10	—	—	—	—	—	—	—
Monument Draw (*ACA*)														
ol	0.20	0.82	0.17	0.90	0.65	0.14	0.14	0.077	0.091	—	0.037	—	0.18	0.015
pig	0.19	0.35	0.35	0.83	—	0.11	0.11	—	0.083	—	—	0.073	—	0.003
aug	0.70	3.30	0.67	3.7	1.4	0.16	1.8	0.34	2.4	0.43	1.4	0.19	1.2	0.19
EET 84302 (*ACA*/*LOD*)														
ol1	—	1.01	0.45	0.61	0.11	0.10	—	—	—	—	—	—	0.10	—
ol2	0.46	0.85	0.62	—	—	0.24	—	—	—	—	—	—	—	—
pig1	—	—	5.1	0.62	0.27	—	0.030	0.011	0.065	0.007	0.064	0.014	0.10	0.032
pig2	0.56	—	0.16	0.63	0.084	—	—	0.010	0.046	0.006	0.070	0.006	0.045	0.022
aug1	2.1	10	1.8	9.4	3.2	0.18	4.0	0.66	4.2	0.79	2.1	0.26	1.5	0.21
aug2	2.6	13	2.2	12	3.9	0.19	5.0	0.83	5.1	0.96	2.5	0.31	1.9	0.28
plag	—	0.95	0.17	—	0.090	—	—	0.005	—	—	0.036	0.024	0.055	0.029
GRA 95209 (*LOD*)														
ol	3.4	0.57	0.39	0.41	0.40	0.12	0.12	0.076	0.090	—	—	—	—	0.009
pig	0.53	1.3	0.23	1.1	0.22	0.20	0.25	0.050	0.33	0.048	0.18	0.042	0.38	0.051
aug	2.0	9.7	1.6	8.3	2.7	0.16	3.4	0.57	3.8	0.67	1.8	0.24	1.5	0.22
LAR 06605 (*LOD*)														
ol1	—	—	—	—	—	—	—	5.1	—	—	—	—	—	—
ol2	—	—	—	—	—	3.2	—	0.067	—	—	—	—	—	—
pig1	—	—	0.17	0.65	0.10	0.13	0.030	0.013	0.020	—	0.040	0.007	0.057	0.022
pig2	—	8.4	0.17	0.65	0.11	0.12	0.031	0.018	0.096	0.012	0.11	0.016	0.11	0.030
aug	0.75	2.5	0.46	2.7	1.0	0.22	1.6	0.30	2.1	0.41	1.2	0.15	1.0	0.15

Note: Minor and trace element mass fractions in $\mu g \cdot g^{-1}$. Mass fractions of REEs in $\mu g \cdot g^{-1}$. Each datapoint represents an average of three analyses of a single mineral grain.
[a]Detection limits for LA-ICP-MS analysis are calculated following the equation of Pettke et al. (2012).

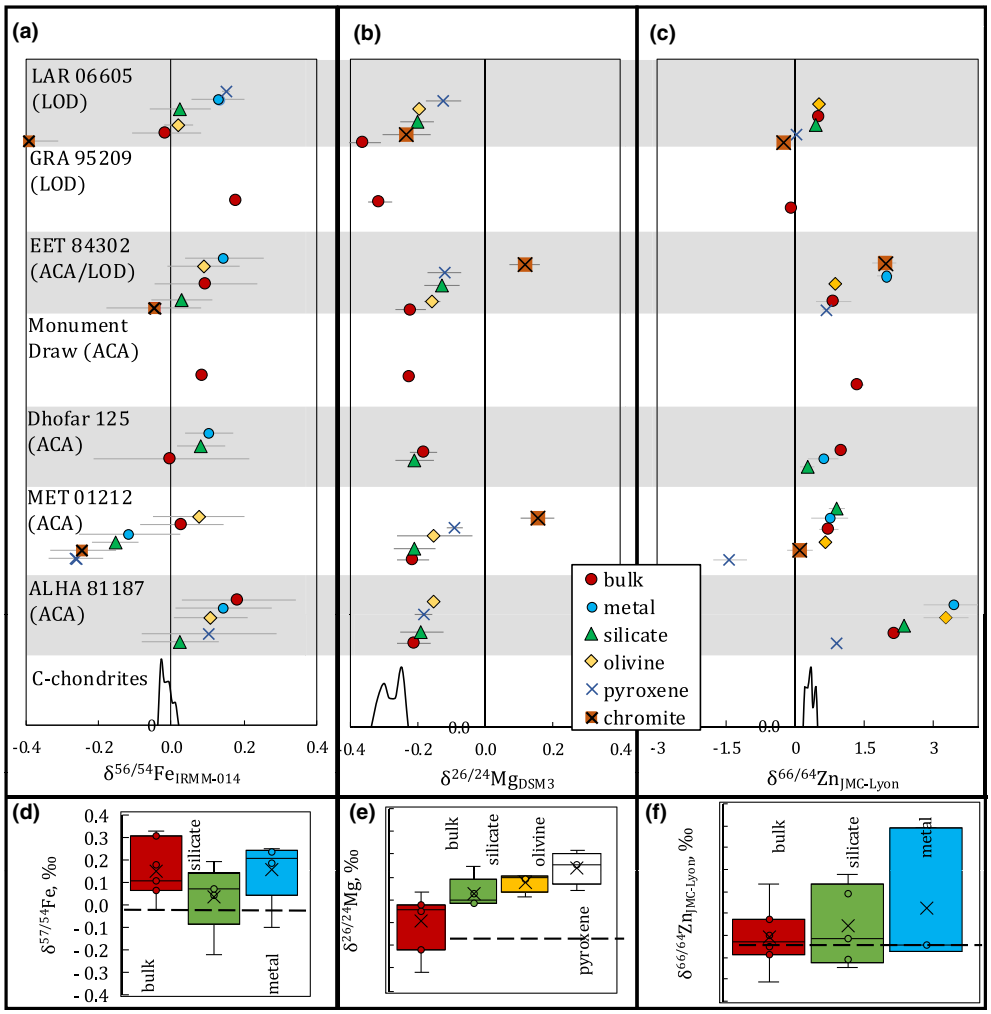

FIGURE 1. Isotopic plots for $\delta^{56/54}$Fe (a), $\delta^{26/24}$Mg (b), and $\delta^{66/64}$Zn (c) values for whole rock ALC meteorites, and their silicate, metal, and mineral separates, measured in this work. The box and whiskers plots (d–f) compare the isotopic compositions of the whole rock, and the major meteoritic reservoirs (i.e., metal and silicate). In the absence of constraints on the exact primordial isotopic reservoir of the ALC parent body, C chondrite isotopic compositions of Zn, Mg, and Fe (Craddock & Dauphas, 2011; Luck et al., 2005; Teng et al., 2010) are shown as a reference for the "average Solar System" as density functions, and the C chondrite average is shown with dashed lines in the box and whiskers plots. (Color figure can be viewed at wileyonlinelibrary.com)

than the known value for the average solar system ($\delta^{56/54}Fe = -0.004 \pm 0.027‰$, SD, based on a compilation of 25 values for carbonaceous (C-) chondrites from multiple publications; Craddock & Dauphas, 2011; Dauphas et al., 2009; Hezel et al., 2010; Poitrasson et al., 2005; Schoenberg & Von Blanckenburg, 2006; Teng et al., 2008; Wang et al., 2013; Zhu et al., 2001). The $\delta^{56/54}$Fe means of ALC and C-chondrites show a significant difference at 95% confidence level with a *p*-value (p) equal to 0.033. At the same time, the mean $\delta^{56/54}$Fe value for whole rock ALC does not display a significant difference compared to the compiled mean of 33 enstatite chondrites at 95% confidence level with $p = 0.053$ ($\delta^{56/54}Fe = 0.005 \pm 0.077‰$, SD, Craddock & Dauphas, 2011; Dauphas et al., 2009; Poitrasson et al., 2005; Schoenberg & Von Blanckenburg, 2006; Zhu et al., 2001). For all the ALC meteorites investigated, the metal reservoir shows a heavier Fe isotopic composition than the corresponding silicate phase (the difference between $\delta^{56/54}Fe_{metal}$ and $\delta^{56/54}Fe_{silicate}$ ranges from +0.02 to +0.12‰; see Table 5). Among all ALC measured, MET 01212 shows the most negative $\delta^{56/54}$Fe values for the metal and silicate components.

The mean $\delta^{26/24}$Mg measured for the bulk ALC ($-0.246 \pm 0.066‰$, SD, $n = 7$) does not differ significantly at the 95% confidence level from the mean value for the average solar system ($-0.280 \pm 0.031‰$, SD, for 13 C-chondrites, Teng et al., 2010; $p = 0.22$), or the measured ALC silicate ($-0.186 \pm 0.035‰$, SD, $n = 5$) with $p = 0.066$. Magnesium isotope ratios for whole rock ALC are significantly lower than those for the pyroxene

TABLE 5. Results of Fe, Mg, and Zn isotope ratio measurements in four acapulcoites, two lodranites, and one transitional acapulcoite/lodranite.

	$\delta^{26/24}$Mg	2SD	$\delta^{25/24}$Mg	2SD	$\delta^{56/54}$Fe	2SD	$\delta^{57/54}$Fe	2SD	$\delta^{66/64}$Zn	2SD
ALHA 81187 (ACA)										
Olivine	−0.149	0.018	−0.076	0.015	0.11	0.10	0.19	0.21	3.29	0.50
Pyroxene	−0.181	0.026	−0.100	0.041	0.10	0.19	0.11	0.56	0.921	0.005
Silicate	−0.187	0.065	−0.109	0.027	0.03	0.11	0.08	0.30	2.393	0.015
Metal	—		—		0.14	0.13	0.25	0.34	3.46	0.67
Whole rock	−0.210	0.049	−0.114	0.042	0.19	0.16	0.32	0.28	2.18	0.10
MET 01212 (ACA)										
Olivine	−0.149	0.112	−0.072	0.082	0.08	0.13	0.09	0.17	0.683	0.001
Pyroxene	−0.090	0.022	−0.044	0.017	−0.26	0.08	−0.20	0.49	−1.41	0.36
Chromite	0.156	0.050	0.077	0.052	−0.24	0.09	−0.32	0.17	0.11	0.28
Silicate	−0.208	0.063	−0.101	0.044	−0.15	0.06	−0.22	0.20	0.91	0.17
Metal	—		—		−0.12	0.14	−0.10	0.24	0.77	0.40
Whole rock	−0.212	0.048	−0.098	0.047	0.03	0.11	0.07	0.10	0.75	0.21
Dhofar 125 (ACA)										
Silicate	−0.208	0.059	−0.119	0.070	0.08	0.07	0.19	0.48	0.28	0.15
Metal	—		—		0.10	0.07	0.23	0.52	0.62	0.34
Whole rock	−0.182	0.042	−0.094	0.052	0.00	0.22	0.06	0.34	1.01	0.12
Monument Draw (ACA)										
Whole rock	−0.224	0.015	−0.099	0.044	0.084	0.014	0.105	0.036	1.37	0.13
EET 84302 (*ACA/LOD transitional*)										
Olivine	−0.155	0.024	−0.084	0.030	0.09	0.10	0.12	0.19	0.87	0.12
Pyroxene	−0.120	0.049	−0.048	0.001	—		—		0.688	0.085
Chromite	0.118	0.044	0.063	0.023	−0.05	0.13	−0.09	0.15	1.96	0.26
Silicate	−0.126	0.053	−0.063	0.056	0.03	0.09	0.07	0.26	1.97	0.17
Metal	—		—		0.15	0.11	0.20	0.24	—	
Whole rock	−0.222	0.044	−0.105	0.048	0.10	0.14	0.18	0.14	0.85	0.39
GRA95209 (*LOD*)										
Whole rock	−0.311	0.037	−0.152	0.014	0.181	0.013	0.30	0.13	−0.056	0.072
LAR 06605 (*LOD*)										
Olivine	−0.193	0.011	−0.105	0.024	0.021	0.039	0.018	0.074	0.551	0.035
Pyroxene	−0.124	0.053	−0.060	0.051	0.152	0.012	0.221	0.065	0.063	0.88[b]
Chromite	−0.230	0.071	−0.112	0.034	−0.390	0.078	−0.60	0.11	−0.23	0.81[b]
Silicate	−0.201	0.051	−0.109	0.037	0.025	0.083	0.04	0.15	0.465	0.032
Metal	—		—		0.129	0.072	0.18	0.18	—	
Whole rock	−0.359	0.051	−0.182	0.030	−0.013[a]	0.094	−0.02[a]	0.14	0.543	0.003
Geological reference materials										
BHVO-2	−0.252	0.080	*−0.094n*	0.050	0.136	0.105	0.118	0.108	0.299	0.065
BHVO-2	−0.217	0.045	*−0.122*	0.050	0.113	0.057	0.139	0.068	0.319	0.076
BHVO-2	−0.187	0.014	*−0.097*	0.019	0.117	0.082	0.174	0.151	0.309	0.027
BCR-1	−0.248	0.148	*−0.097*	0.079	0.119	0.025	0.144	0.064	0.250	0.013
JP-1	−0.159	0.063	*−0.082*	0.047	−0.007	0.128	−0.040	0.250	0.659	0.289
JP-1	−0.225	0.091	*−0.113*	0.050	0.053	0.040	0.109	0.083	—	—
JB-1b	—	—	—	—	0.065	0.044	0.147	0.050	—	—

Note: The data are presented as delta notation in‰ relative to the isotopic reference material indicated. The intermediate precision is presented as 2SD of replicate measurements ($n = 3$–5) carried out in a period of several days.

[a]Due to an interference on $m/z = 54$, $^{57}Fe/^{56}Fe$ was used to calculate both $\delta^{56/54}$Fe and $\delta^{57/54}$Fe, assuming mass-dependent effects only.

[b]2SD of a single measurement (repeatability) is reported, because of the low amount of Zn available.

($\delta^{26/24}Mg_{px} = -0.129 \pm 0.038‰$, SD, $p = 0.004$) or olivine ($\delta^{26/24}Mg_{oliv} = -0.162 \pm 0.021‰$, SD, $n = 4$, $p = 0.013$) separates at 95% confidence level. While the Mg isotopic composition was not measured in the plagioclase, metal, or sulfide components, these should explain the significant difference between the pyroxene/olivine and bulk ALC. Plagioclase was not analyzed due to the technical challenges associated with extracting it, and metal because it is expected to have low Mg content. The $\delta^{66/64}Zn$ values for all ALC meteorites ($\delta^{66/64}Zn$ from −0.06 to 2.18‰) except that for GRA 95209 lodranite are significantly higher than those reported for C-chondrites (Luck et al., 2005). The >2‰ spread of the $\delta^{66/64}Zn$ values found in the ALC meteorites is a feature not typical for chondrites and is more characteristic for differentiated achondrites (Moynier et al., 2010; Paniello, Day, & Moynier, 2012).

The accessory chromite minerals of ALC have distinct Fe and Mg isotopic compositions. The $\delta^{56/54}Fe$ values for the chromite in LAR 06605, EET 84302 and MET 01212 are $-0.390 \pm 0.078‰$, $-0.05 \pm 0.13‰$, and $-0.243 \pm 0.089‰$, respectively, which is lower (isotopically lighter) than the values for the bulk meteorites. The $\delta^{26/24}Mg$ values are $-0.230 \pm 0.071‰$, $0.118 \pm 0.044‰$, and $0.156 \pm 0.050‰$, respectively, which is isotopically heavier than those for the corresponding whole rock meteorite samples. However, evaluation of the polished sections indicated that chromite is an accessory mineral and as such, it likely has no significant effect on the Fe and Mg isotopic compositions of bulk meteorites.

DISCUSSION

Nuclide Accretion from the Nebula

Overall, primitive meteorites are characterized by rather narrow distribution of Fe isotopic signatures (Craddock & Dauphas, 2011). The $\delta^{56/54}Fe$ results of whole rock ALC ($-0.080 \pm 0.081‰$, SD, $n = 7$) are statistically significantly higher than CC ($-0.004 \pm 0.027‰$, SD, $n = 25$, with p-value 0.033) and ordinary chondrites (OC, $-0.012 \pm 0.048‰$, SD, $n = 38$, with p-value 0.022) are an unexpected find (see Figure S9). At the same time, because the Fe isotopic signatures of the enstatite chondrites (EC, $\delta^{56/54}Fe = 0.005 \pm 0.077‰$, SD, data on 33 EC compiled from Craddock & Dauphas, 2011; Dauphas et al., 2009; Poitrasson et al., 2005; Schoenberg & Von Blanckenburg, 2006; Wang et al., 2014; Zhu et al., 2001) have a larger dispersion compared to CC or OC, the difference of the mean values of the EC and ALC is not statistically significant at the 95% confidence level, with a p-value of 0.053 (yet significant at the 90% confidence level). As such, due to the higher dispersion of the $\delta^{56/54}Fe$ values, the EC reservoir may potentially be more suited to represent the parent material of the ALC meteorites. However, clearly more data are needed on ALC meteorites to verify this hypothesis.

Alternatively, however, the superchondritic Fe isotopic signatures of the ALC may result from a differentiation process (see discussion in the following sessions). Different to Fe, the Mg isotopic signatures of ALC ($\delta^{26/24}Mg = -0.246 \pm 0.064‰$, SD, $n = 7$) do not differ significantly from the composition of chondritic reservoirs reported in Teng et al. (2010) with $\delta^{26/24}Mg$ of CC $= -0.283 \pm 0.020‰$, SD ($n = 8$), $\delta^{26/24}Mg$ of OC $= -0.287 \pm 0.020‰$, SD ($n = 19$), or $\delta^{26/24}Mg$ of EC $= -0.282 \pm 0.022‰$, SD ($n = 10$; see Figure S9). Both the Fe and Mg isotope ratio data for the ALC meteorites analyzed exhibit a range significantly broader than that for any chondritic reservoir (Figure S9). These ranges are wider than what can be attributed to the measurement reproducibility. As such, this heterogeneity could have been inherited from the unknown primordial material, for example, controlled by disproportional amounts of chondrules, which underwent episodes of evaporation and condensation in the nebula (Wang et al., 2013).

On the other hand, stable isotopic signatures are less useful in tracing the origin of meteoritic reservoirs compared to nucleosynthetic or radiogenic isotopes due to their susceptibility to fractionation during differentiation processes. Zn isotopes are especially unlikely to record the original isotopic ratios of the primordial reservoir, due to its high susceptibility to fractionation under planetary differentiation conditions. As the mean Fe isotopic signatures of the ALC's PB seem to be marginally higher than the potential primary OC reservoir and more similar to the EC reservoir, it might be interpreted to result from low degree melting and metamorphism (see further discussion). Only Mg isotopes appear to have preserved the original chondritic signature of the ALC's PB.

A large spread in the oxygen isotopic signatures of ALC ($\Delta^{17}O = -1.12 \pm 0.36‰$), broadly correlated with mafic silicate compositions, suggests that the ALC PB initially accreted from non-homogenous nebular components (Dhaliwal et al., 2017; Greenwood et al., 2017). Although no significant variations of the nucleosynthetic anomalies of, for example, Cr or Ti can be resolved within the ALC PB (Rüfenacht et al., 2023), it is important to know whether stable isotope ratio signatures can record nebular inhomogeneity during the ALC accretion or not. Indeed, if the oxygen isotopes did not experience a sufficient temperature rise and time during the episode of low-degree of partial melting, melt migration, and pooling to completely equilibrate and form a well-defined linear fractionation array in the

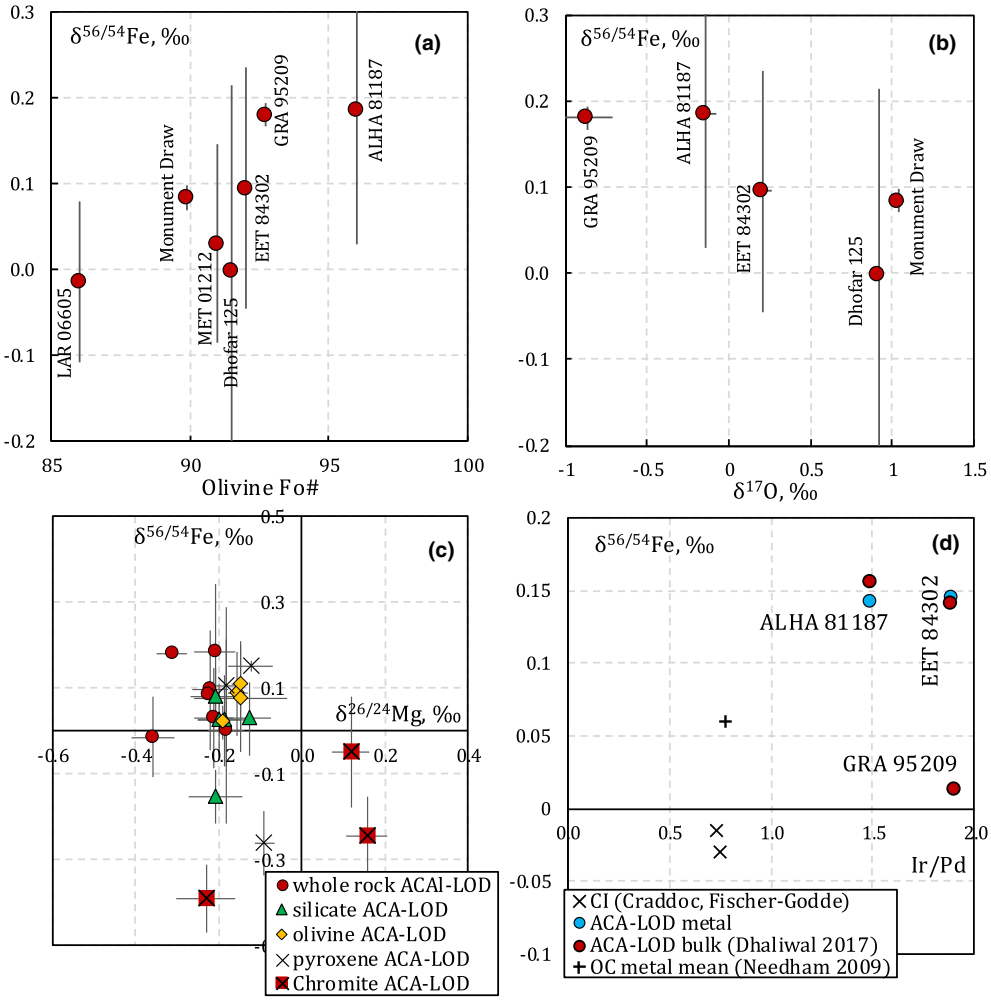

FIGURE 2. Plots of $\delta^{56/54}$Fe values for acapulcoite lodranite meteorites (this study). (a) $\delta^{56/54}$Fe values for the whole rock meteorites show a weak correlation to their olivine compositions (Keil & McCoy, 2018). (b) $\delta^{56/54}$Fe values for the whole rock meteorites show a weak anti-correlation to their oxygen isotopic composition (Greenwood et al., 2017). (c) Absence of anti-correlation between $\delta^{56/54}$Fe and $\delta^{26/24}$Mg values for the whole rock meteorites and their silicate and mineral separates suggests that diffusive kinetic equilibration had no effect on the isotopic signatures. (d) $\delta^{56/54}$Fe values for the whole rock meteorites and their metal fractions (this study) show no covariation with their Ir/Pd ratios (Dhaliwal et al., 2017). Data for CI and ordinary chondrites (Craddock & Dauphas, 2011; Fischer-Gödde et al., 2010; Needham et al., 2009) are shown for comparison. (Color figure can be viewed at wileyonlinelibrary.com)

δ^{18}O–Δ^{17}O space, it is reasonable to expect that the far less mobile elements Zn, Fe, and Mg preserve their pristine nebular isotopic signatures.

Figures 2b and 3b plot $\delta^{56/54}$Fe and $\delta^{66/64}$Zn values for bulk ALC meteorites versus their δ^{17}O values (Greenwood et al., 2017). A similar plot can be found for Mg in Figure S2, and $\delta^{56/54}$Fe, $\delta^{66/64}$Zn, and $\delta^{26/24}$Mg plots versus Δ^{17}O and δ^{18}O in Figure S6. No covariation of the $\delta^{66/64}$Zn or $\delta^{26/24}$Mg values with the oxygen isotopic composition is observed (Figure 3b and Figure S2b). Similarly, $\delta^{66/64}$Zn and $\delta^{26/24}$Mg do not covary with the Fa# of the olivine (Figure 3a and Figure S2a). The absence of a visible mixing array can result from (i) a homogenous composition of the nebula components at the time of the ALC's PB accretion, or (ii) melt mobility and complex pooling in the different zones of the ALC's PB, obliterating any potential mixing lines that could have been present in the PB before the differentiation, or be due to (iii) a non-representative number of samples. In the absence of correlation between the isotope ratios of O and those of Zn and Mg, the ALC's PB accretion from primordial nebular components with homogenous isotopic compositions should be considered more likely than that the correlation was initially present but later became erased following differentiation processes. However, analysis of a higher number ALC meteorites and simultaneous measurements of the nucleosynthetic Zn isotopic anomalies would likely provide a more definitive answer.

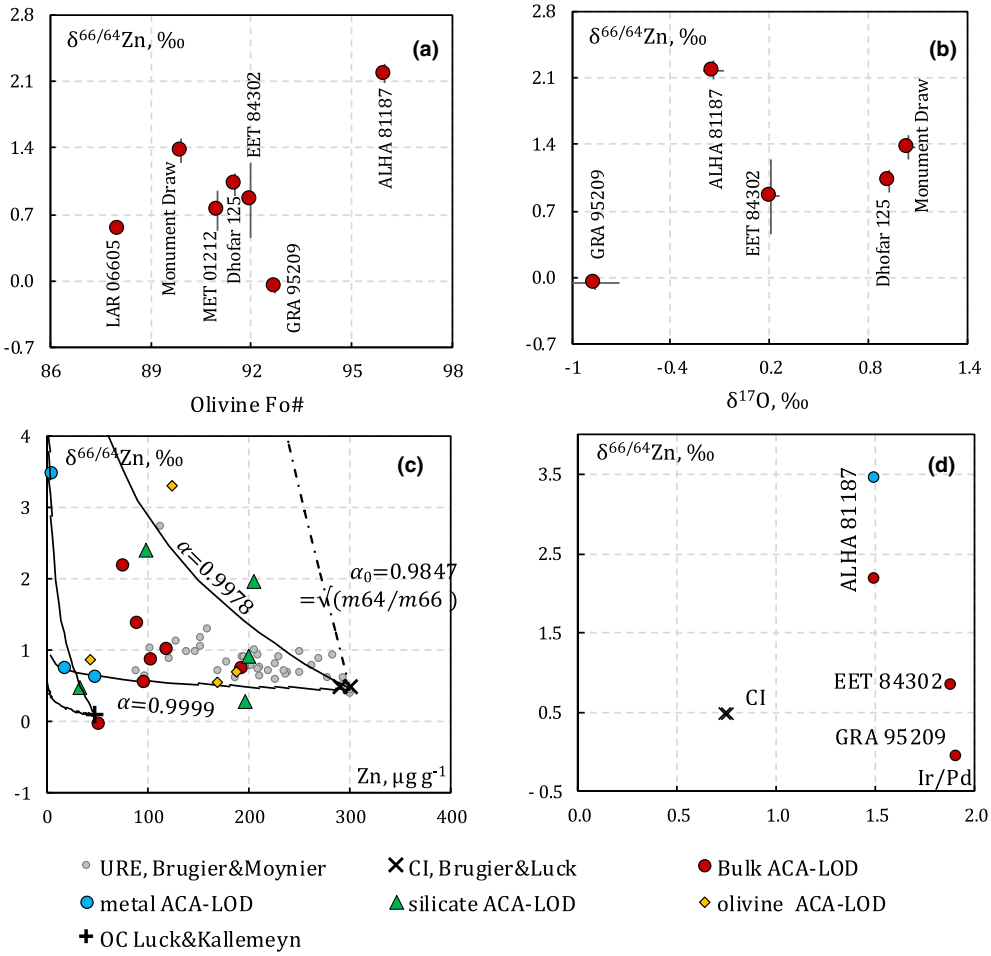

FIGURE 3. Plots of $\delta^{66/64}$Zn values for ALC (this study). (a) $\delta^{66/64}$Zn values for the whole rock meteorites show no covariation with their olivine compositions (Keil & McCoy, 2018). (b) $\delta^{66/64}$Zn values for the whole rock meteorites show no covariation with their oxygen isotopic composition (Greenwood et al., 2017). (c) Diagram of $\delta^{66/64}$Zn values for whole rock ALC meteorites and their components plotted versus their Zn mass fractions. The black lines model the Zn isotope signatures in case of Zn loss and isotopic fractionation according to a Rayleigh process with fractionation factors from 0.9978 to 0.9999. A Rayleigh process with a fractionation factor corresponding to ideal evaporation to vacuum $\left(\sqrt{(m_{64}/m_{66}} = 0.9847\right)$ is shown with a dashed line. Literature data for chondrites are from Brugier et al. (2019); Kallemeyn et al. (1989); Luck et al. (2005). Ureilites—another group of achondrites thought to have undergone Zn isotope fractionation during the process of Zn loss—are shown with gray markers (Brugier et al., 2019; Moynier et al., 2010). (d) $\delta^{66/64}$Zn values for the whole rock meteorites and their metal fractions show no covariation with their Ir/Pd ratios (Dhaliwal et al., 2017). Data for CI and ordinary chondrites (Fischer-Gödde et al., 2010; Luck et al., 2005) are shown for comparison. (Color figure can be viewed at wileyonlinelibrary.com)

The plot of $\delta^{56/54}$Fe values for bulk ALC meteorites versus their δ^{17}O and olivine Fa# values (Figure 2a,b) shows a covariation (Pearson's correlation coefficient of −0.84). However, this mixing line is based on five meteorite datapoints only, for which both Fe and O isotopic compositions are known, and no covariation of Fe isotope ratios with Δ^{17}O is observed. Moreover, the fact that $\delta^{56/54}$Fe has a negative correlation coefficient with δ^{17}O and δ^{18}O, and a positive correlation coefficient with the olivine Fa#, does not match the positive correlation between the O isotopes and olivine Fa# known for the ALC (Keil & McCoy, 2018). As such, while the observed mixing line between Fe isotope ratios and δ^{17}O (and δ^{18}O) in ALC meteorites preliminarily suggests a potential formation of the PB from primordial nebula components with different Fe isotopic compositions, it should likely be interpreted as a coincidental trend due to limited number of datapoints. More analyses are needed to confirm whether the Fe isotopic signatures of the ALC species analyzed truly reflect isotopic inhomogeneity in the early Solar Nebula.

Isotope Thermochemistry

The two pyroxene thermometry measurements of Lucas et al. (2022) resulted in 948–1034°C equilibration

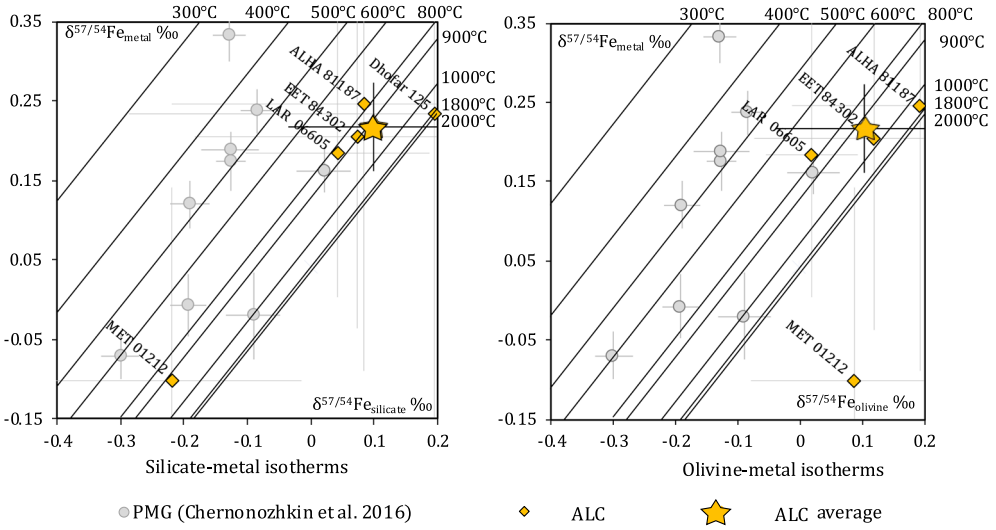

FIGURE 4. $\delta^{57/54}Fe_{metal}$ versus $\delta^{57/54}Fe_{olivine}$ plot for the ALC meteorites. The compilation of metal and silicate data for main group pallasites (PMG, Chernonozhkin et al., 2016), for which metal and olivine reservoirs are out of equilibrium, as they might originate from different parent bodies, are shown with gray markers. The isotherms are calculated using the NRIXS parameters for γ-iron and olivine equilibration (Dauphas et al., 2012, 2014). (Color figure can be viewed at wileyonlinelibrary.com)

temperatures for acapulcoites, 965–1108°C for transitional acapulcoite–lodranites, and somewhat higher 941–1114°C temperatures for lodranites. These values are interpreted to record a progressive increase of peak equilibration temperatures with burial depth toward the center of the internally heated primordial ALC PB. These temperatures are broadly consistent with the range of the pyroxene thermometry results for two ALC meteorites in this work (983 and 1036°C; Table 3). The 60°C temperature difference for the LAR 06605 lodranite, compared to 1047°C obtained by Lucas et al. (2022), might reflect the variation of the temperature value obtained for different hand specimens as a result of melt infiltration and melt-rock back reactions. Alternatively, the discrepancy could result from the fact that the measured pyroxene grains are not in direct contact with each other, as metal appears to have been completely molten and injected interstitially between subrounded silicate grains. Even though the individual silicate grains do not show chemical zoning due to redox reactions with the metal melt, they might have recorded this metal silicate re-equilibration event. Overall, application of different thermometry methods (REEs in 2-pyroxene and Ca in olivine) records rapid cooling from peak temperatures at several °C per year, and thermal modeling suggests a collisional fragmentation event, which ceased the PB differentiation (Lucas et al., 2022).

Fe isotopic signatures in ALC silicate are isotopically lighter than in the metal reservoir (a difference between $\delta^{56/54}Fe_{metal}$ and $\delta^{56/54}Fe_{silicate}$ of 0.023–0.117‰), which is in line with the first-order predictions by thermodynamic constraints for smaller bodies (Elardo et al., 2019; Johnson et al., 2020). They also agree with the observations for the Fe isotopic composition in equilibrated metal and silicate reservoirs in the solar system (e.g., iron meteorites, chondrites; Poitrasson, 2007; Weyer et al., 2005), as well as pallasites, which are believed to be non-equilibrated mixtures of metal and olivine (Bennett et al., 2022; Chernonozhkin et al., 2017; Zhu et al., 2001). This direction of isotope fractionation in the silicate–metal system is in agreement with the Fe isotope ratio thermometer, presented in Figure 4 as a plot of $\delta^{57/54}Fe_{metal}$ versus $\delta^{57/54}Fe_{olivine}$, together with the isotherms for γ-iron–olivine equilibration calculated using the NRIXS parameters of Dauphas et al. (2012, 2014). Both handpicked olivine versus metal and silicate versus metal plots are shown. While the bulk metal is in contact with different silicate minerals, the bulk silicate versus metal type of plot approximates that combined silicate has its Fe isotopic signature close to that of olivine, as olivine is the major component of the ALC silicate. The ALC meteorites fall on Fe isotherms with temperatures of 800–950°C, broadly comparable to the 836–1036°C equilibration temperatures calculated by the pyroxene geothermometer (Table 2). Among the ALC meteorites measured, MET 01212 exhibits the most negative $\delta^{56/54}Fe$ values, and yields an unrealistic equilibration temperature when olivine–metal isotherms are considered. This may be the result from oversampling of sulfides or pooling of evolved metal melt, which is not in equilibrium with the silicate characterized. While the precision of the equilibration temperatures based on Fe isotope thermometry cannot compete with those obtained

by of the traditional pyroxene method, these results suggest that Fe has essentially reached isotopic equilibrium between the reservoirs of the ALC PB.

Absence of Isotope Fractionation by Low Degree of Partial Melting and Melt Separation Processes

Isotope ratios of non-traditional stable isotopic systems can be fractionated by various planetary differentiation processes, and the ALC provide a perfect case to understand whether or not Fe, Mg, and Zn isotopes are fractionated in the process of low-degree partial melting. Unfortunately, the primitive isotopic composition of the ALC PB is not known, and moreover, ordinary and enstatite chondrites exhibit a very narrow range of Fe and Mg isotopic signatures, preventing the use of Fe and Mg stable isotope ratios to characterize potential primordial reservoir of ALC. As such, it is difficult to evaluate whether any difference of the isotopic composition between the ALC meteorites and their hypothetical primordial material (or absence of such difference) is the result of low-degree melting. However, knowledge of trace element behavior during melting provides an alternative approach; here, the acquired data set was examined for correlation between the Fe, Mg, and Zn isotopic signatures and known geochemical tracers of partial melting. For example, the plots of the Zn mass fraction versus the FeO content (Figure 3a) and versus the conservative refractory element Sc in silicate minerals (Figure 5a,b) demonstrate higher affinity of Zn toward olivine and pigeonite in ALC meteorites. It hints toward potential isotope fractionation during partial melting of plagioclase and augite, and it should be verified whether the early separation of silicate and Fe-FeS melts can cause isotope fractionation.

Several element proxies for melt mobility can be used to identify a potential correlation with the isotope ratios. First, REE mass fractions reflect the complex nature of partial melting and silicate melt migration at the ALC PB (Figure 6b,c), where different proportions of basaltic melts could have been mobilized from the rocks and pooled in other regions of the PB (Dhaliwal et al., 2017; McCoy et al., 1997), or even were completely removed from the primordial PB by impact processing or volcanism. The results of light REE measurements in orthopyroxene and especially in olivine in this work are likely affected by measuring close to the detection limits, as well as by terrestrial weathering under the dry desert or Antarctic conditions. Nevertheless, as the augite REE mass fractions are significantly higher, they reproduce earlier observations (e.g., Floss, 2000). Chondrite-normalized Sm and Dy mass fractions in augite have a strong positive correlation (Figure S3) as a result of REE extraction. However, no systematic differences between acapulcoites, lodranites, and transitional members are observed, likely as a result of complex pooling (McCoy et al., 1996). Figure S4 demonstrates absence of visible co-variation of Fe, Mg, and Zn isotopic signatures with the chondrite-normalized Sm concentration in augite.

Also, clues of igneous processes can be inferred from the Fe-Mg-Mn relations (Figure 5c). While the absence of strong horizontal trends at constant Fe/Mn, more typical for evolved achondrites (Goodrich & Delaney, 2000) points toward an absence of significant igneous processes, low-degree partial melting, melt mobilization, and pooling result in minor dispersion of the initial Mn/Mg ratios within the chondritic range. Augite minerals of ALC have near-identical Mn/Mg ratios, and the super-chondritic (Goodrich & Delaney, 2000) slope can be interpreted as an indication of partial melting of augite. The trend of data for ALC meteorites toward the origin in the Fe/Mg-Fe/Mn space has been suggested earlier to record primordial heterogeneity in the nebula materials, from which the ALC PB had accreted (Goodrich & Delaney, 2000). Alternatively, we suggest that for augite in ALC meteorites, this Fe loss/gain trend records re-equilibration of high-Ca pyroxenes with different Fe mass fractions at variable peak temperatures within the PB, plagioclase–clinopyroxene (basaltic) melt mobilization and pooling. A large range of high-Ca clinopyroxene Fs# compositions from 2.1 to 13 had been recorded by Keil and McCoy (2018). Although the Fe/Mn ratio in augite seems to be a potent marker of melt mobility, no covariation is found between the Fe/Mn ratio and Fe, Mg, or Zn isotopic signatures (Figure S5).

As such, REE and Fe-Mg-Mn compositions of silicate minerals suggest that the Fe, Mg, and Zn isotopic signatures of ALC meteorites are not affected by the low degree of partial melting of silicates and melt separation within the ALC's PB. Similarly, Fe and Mg isotopic signatures in ALC meteorites are not governed by a kinetic isotopic effect due to diffusion between minerals, because in that case, a negative correlation would be observed between Mg and Fe isotopic compositions for bulk ALC samples, and their silicate and olivine separates, which is not the case (Figure 2c).

The two lodranites measured have the lightest Zn isotopic signatures among the seven meteorites studied in this work. It is known that, among the ALC meteorite types, lodranites have higher degrees of metal melt separation, and therefore lighter Zn isotopic signatures, which can be potentially explained as a result of removal of the isotopically heavy sulfides with the early metal melts (i.e., Pringle et al., 2017). However, when Fe and Zn isotopic signatures of the whole rock meteorites and the metal separates are compared to the Ir/Pd ratios of the bulk meteorites (data from Dhaliwal et al., 2017), no covariation is observed (Figures 2d and 3d). As such,

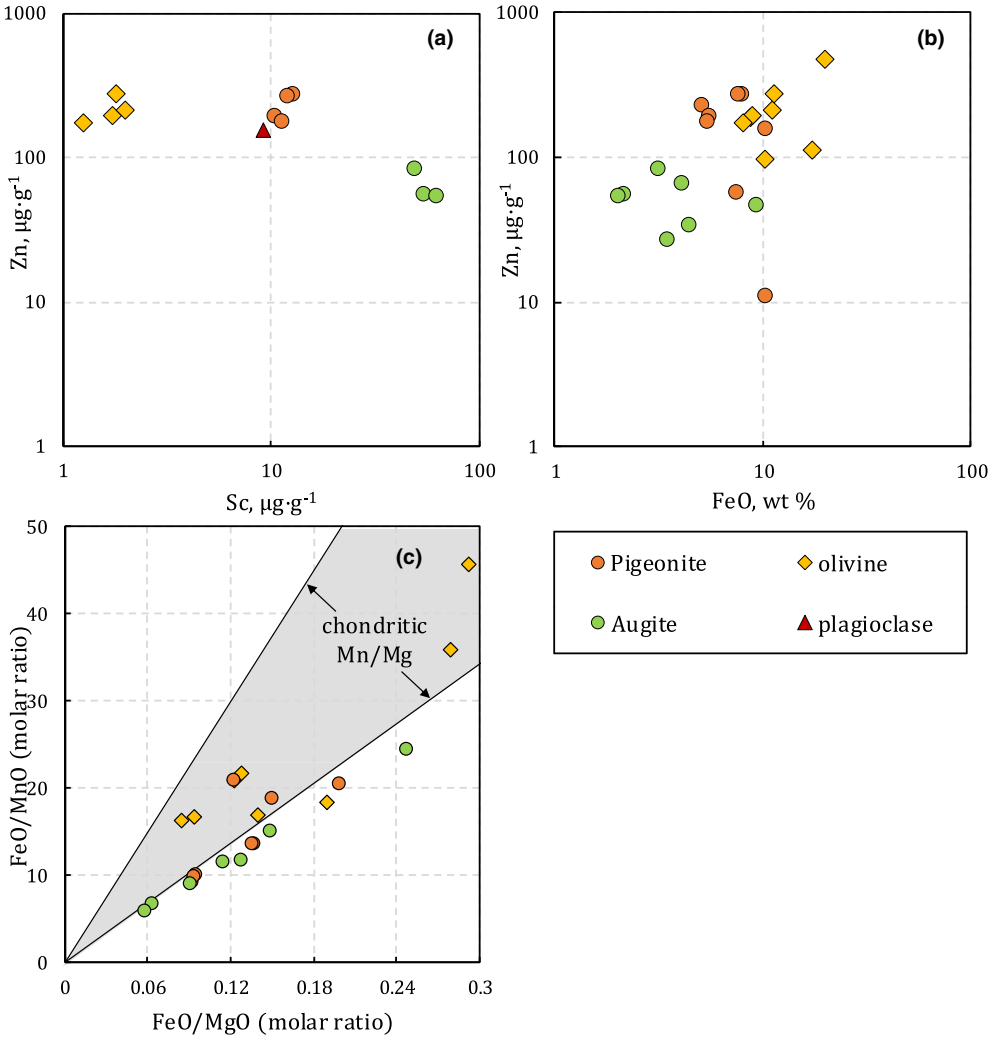

FIGURE 5. (a) LA-ICP-MS results for Zn plotted versus the fraction of conservative refractory Sc in silicate minerals of acapulcoite lodranite meteorites. (b) LA-ICP-MS results for Zn in silicate minerals of acapulcoite lodranite meteorites plotted versus their FeO data. Each datapoint represents an average composition obtained from multiple analyses of a single mineral grain. The plots suggest potential Zn fractionation during partial melting and melt migration. (c) plot of molar Fe/Mg ratio versus Fe/Mn ratio for silicate minerals of ALC meteorites adapted from Goodrich and Delaney (2000). The linear tends toward the origin at a constant Mn/Mg ratio reflect Fe loss/gain processes. The augite shows slightly super-chondritic Mn/Mg ratios, suggesting that they are affected by low-degree partial melting. (Color figure can be viewed at wileyonlinelibrary.com)

the present work found no evidence for the early extraction of Fe-FeS melts fractionating the isotopes of Fe and Zn within the ALC PB.

Isotope Fractionation by Evaporation

As our data provide no evidence for Zn isotope fractionation in ALC meteorites neither by PB early differentiation processes, nor for it being inherited from the nebula, we suggest that the evaporation is the most viable explanation for the Zn isotopic signatures observed for some ALC species shifted toward heavier values (compared to OC and CC) and lower Zn mass fractions, recorded at Figure 3c. Figure 6a shows the CI-normalized element mass fractions in the silicate minerals of ALC meteorites, arranged according to their volatility in the nebula. Although most lithophile elements are somewhat enriched in the minerals compared to CI, the elements with lower 50% condensation temperatures, for example, Cr and Mn (1296 and 1158°C, respectively) are depleted as a result of evaporative loss. The moderately volatile elements Cu, Pb, and Zn, which tend to demonstrate chalcophile properties, show an even higher depletion. However, this can be alternatively explained by losses as a result of eutectic Fe-FeS melting and melt mobility, as is obviously the case for Co and Ni, which

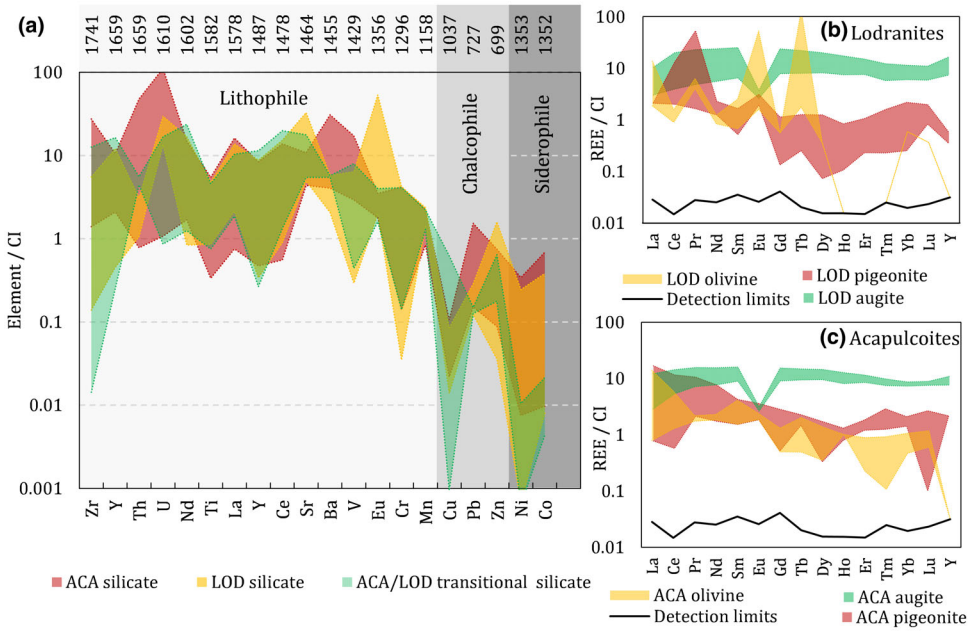

FIGURE 6. CI chondrite normalized results of trace element measurements in olivine and pyroxene of acapulcoite–lodranite meteorites as determined with LA-ICP-MS. The limits of detection, calculated using the approach of Pettke et al. (2012), are shown with the black line. The CI normalization values of REE are from Dauphas and Pourmand (2015) and from Barrat et al. (2012) for all other elements. This volatility plot demonstrates no significant difference between acapulcoites, lodranites, and the transitional acapulcoite-lodranite meteorite. (a) Elements arranged according to their 50% condensation temperature (Lodders, 2003). (b) REE patterns of silicate minerals in lodranites. (c) REE patterns of silicate minerals in acapulcoites. (Color figure can be viewed at wileyonlinelibrary.com)

are siderophile at the PB conditions. Here, stable isotope ratio signatures of the moderately volatile element Zn provide an additional perspective, as isotope fractionation of moderately volatile elements is known to occur during incomplete evaporation in solar system processes (Paniello, Day, et al. 2012; Sossi et al., 2016), as well as in planetary differentiation processes, albeit to a smaller extent.

The depletion of moderately volatile elements can result from incomplete condensation of the solar nebula. However, in the case of incomplete condensation from the nebula, a correlation of $\delta^{66/64}$Zn with the oxygen isotopic composition would be generally expected, which is not found (Figure 3b). Moreover, the experiments of Collinet and Grove (2020) suggest that small parent bodies in the inner solar system were initially not depleted in moderately volatile alkali elements. As such, the moderately volatile element fractions (and isotopic composition of Zn) are likely to be affected by evaporation processes during heating of the PB (Dhaliwal et al., 2018).

Figure 3c shows $\delta^{66/64}$Zn values for the ALC meteorites and their metal, silicate, and mineral separates, plotted versus the corresponding Zn mass fractions. The data demonstrate overall heavy Zn isotopic compositions with decreasing Zn mass fractions. In previous work, isotopically heavy Zn and low Zn mass fractions had been observed in other meteorite groups (e.g., ureilites, lunar meteorites, CB, and CH chondrites) and these results were interpreted to reflect evaporative loss (Moynier et al., 2010; Paniello, Day, et al., 2012; Pringle et al., 2017). Importantly, all measured fractions of ALC (silicate and metal reservoirs, olivine separates) show isotopically heavy signatures, which precludes the metal differentiation scenario of Zn isotope fractionation in ALC meteorites, and hints toward evaporation being the controlling process. The Rayleigh evaporation model lines with different fractionation factors α are shown in Figure 3c with black solid lines, and the ideal evaporation to vacuum with a dashed line. Because nucleosynthetic anomalies and other parameters preclude ALC PB formation from any known chondritic material, so that the origin of the primordial material of the ALC PB is currently not known, multiple potential starting points for the Rayleigh model are shown (Barrat et al., 2012; Kallemeyn et al., 1989; Luck et al., 2005).

Several outcomes can be derived from the Zn data for the ALC meteorites. Firstly, the lightest Zn isotopic compositions of the ALC meteorites and their components (e.g., bulk GRA 95209 lodranite −0.056‰, chromite in MET 01212 and LAR 06605, and pyroxene in LAR 06605; see Table 5) record primordial ALC Zn isotopic signatures more similar to those of

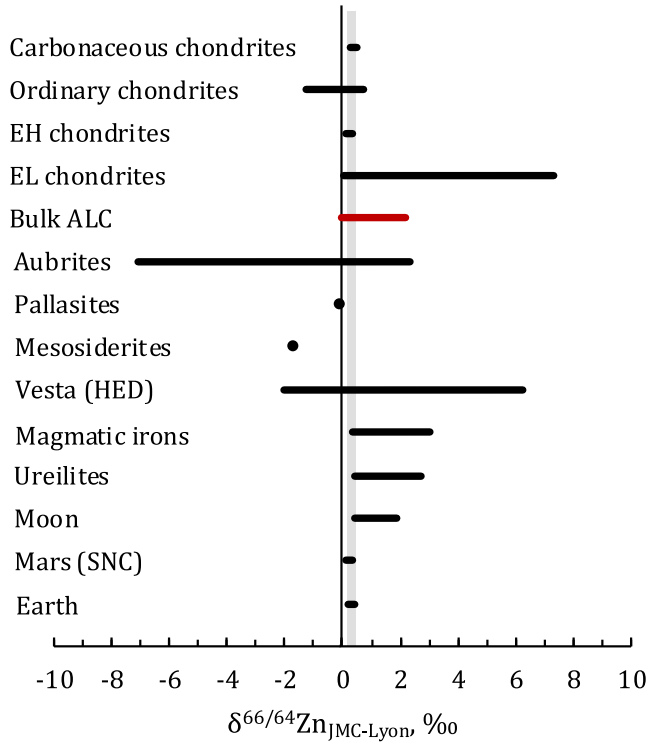

FIGURE 7. Comparison of the $\delta^{66/64}$Zn values of bulk ALC meteorites with the Earth signatures (gray bar) and other meteorite groups. Enstatite chondrites and aubrites—Moynier et al. (2011), HED—Paniello, Moynier, et al. (2012), Moon—Paniello, Day, et al. (2012), carbonaceous and ordinary chondrites—Luck et al. (2005), ureilites—Brugier et al. (2019), iron meteorites—Bridgestock et al. (2014). (Color figure can be viewed at wileyonlinelibrary.com)

unequilibrated ordinary chondrites $\delta^{66/64}$Zn from −0.4 to 0.5‰ (Luck et al., 2005) in the inner solar system (Figure 7). If evaporation from a single homogenous Zn sink is the only process driving the Zn signatures, the plot suggests that the primordial material of the ALC PB showed higher Zn concentrations than those found for any chondrite (CI—312, OC—47, EH—250 μg g^{-1}; Wasson & Kallemeyn, 1988). Likely, Zn in ALC PB originated from a reservoir that is not identified among chondrites. Secondly, the ALC data do not fall on the model of ideal evaporation to vacuum, as is also the case for other meteorite groups, for which evaporative loss of Zn is suggested. Moynier et al. (2010) suggested it to be a result of the evaporation regime, where the escape of Zn isotopes is limited by diffusion to the surface layer of the PB. This can similarly be the case for the layered ALC PB, where the outer layers of the PB reached overall lower peak temperatures compared to its central regions, further limiting the diffusion of Zn (Li et al., 2018; Lucas et al., 2022).

Finally, it can be observed that the overall magnitude of Zn isotopic fractionation of the ALC, for which the thermal evolution of the PB ceased before reaching the magma ocean stage, is comparable with that of the other differentiated planetesimals, which are believed to have lost Zn as a result of evaporative processes (Figure 7). For example, the $\delta^{66/64}$Zn values of the Moon span from 0.46 to 1.9‰, resulting from the giant Moon-forming impact (Paniello, Moynier, et al., 2012). At the same time, asteroid 4 Vesta, represented by the howardite, eucrite, diogenite (HED) meteorites group, which is also believed to have its Zn isotopic signatures affected by impact-related evaporation in the early solar system, as well as by mixing with lighter chondritic components, has a significantly larger span of $\delta^{66/64}$Zn values (−2 to 6.22‰, Figure 7). The Zn isotopic systematics of the ALC indicate that the Zn evaporation processes in the solar system may occur even prior to the magma ocean stage of planetesimal evolution, for example, due to low escape velocities of smaller PBs, such as that of ALC meteorites.

On the other hand, caution is required when interpreting evaporative Zn isotopic signatures, as fractionation mechanisms in the nebula remain poorly understood, which is underlined by the broad range of Zn isotopic signatures within chondrites (Figure 7; Luck et al., 2005). In addition, Zn isotopes on differentiated parent bodies are known to fractionate during metal differentiation and core formation processes (e.g., in magmatic irons; Bridgestock et al., 2014). Although the observed absence of correlation between the Zn isotopic signatures and O isotope ratios and trace element proxies for differentiation of ALC meteorites cancels out any scenarios of Zn fractionation in nebular or planetary differentiation processes (and leaves evaporation as the most likely process), more convoluted pathways could also result in heavy Zn isotopic signatures.

CONCLUSIONS

This work presents the first comprehensive data set of Fe, Mg, and Zn stable isotope ratios for the acapulcoite lodranite meteorite clan, supported by their elemental mineral compositions, which allow further conclusions concerning the processes potentially resulting in the isotope fractionation patterns observed to be drawn. Iron, Mg, and Zn isotope ratios for seven bulk ALC meteorites as well as for their metal, silicate, and mineral separates provide a perspective on the meteorite petrogenesis complimentary to the reconstructed PB histories as unraveled based on their petrology, major and trace element systematics, radionuclide geochemistry, and nucleosynthetic anomalies.

The isotopic signatures of Zn and Mg in ALC meteorites do not correlate with the oxygen isotope ratios, which are believed to record nebular processes.

Although the Fe isotopic signatures for bulk ALC meteorites, for which O isotopic compositions are known, show covariation with their $\delta^{17}O$ and $\delta^{18}O$ values, more data are needed to confirm whether the $\delta^{56/54}Fe$ values are inherited from the primordial materials before accretion, and whether the ALC PB has recorded Fe stable isotope heterogeneity in the nebula.

No isotopic and element data presented in this work suggest that the Fe, Mg, and Zn isotopic compositions could have been affected by the early planetary differentiation processes. Platinum group elements (PGE) are known to be an excellent marker of solid–liquid metal differentiation and metal-sulfide melt mobility at differentiated planetesimals. Our results show no covariation of the PGE proxies of the metal–sulfide melting with the Fe and Zn isotopic signatures. If extraction of metallic melts was at the origin of the isotope fractionation of Zn and Fe (which tend to be chalcophile and siderophile under certain conditions), covariation of their isotopic signatures with PGE levels could be expected. As such, the fractionation of Fe and Zn isotope ratios during metal–sulfide melting cannot be invoked. Similarly, the REE and Fe-Mg-Mn relations in augite, which record low-degree partial melting of silicates and plagioclase–clinopyroxene (basaltic) melt mobility within the PB, do not covary with the Fe and Zn isotopic signatures, precluding Fe and Zn isotope fractionation during low-degree of silicate partial melting.

As there is no evidence that the Zn isotopic composition records low-degree partial melting, this work suggests that the overall heavy highly variable Zn isotopic compositions are a result of Zn evaporation. Absence of correlation between Zn and O isotopic compositions does not completely preclude this evaporation happening at the nebular stage, as oxygen isotopic signatures can be easily convoluted by silicate melt mobility and pooling. Moreover, the initial Zn isotopic composition in the early solar system is not clear, further complicated by Zn heterogeneity in the nebula, supported by the discovery of Zn nucleosynthetic dichotomy. Alternatively, the Zn evaporation from the ALC meteorites may be of impact origin, although the results of this work do not allow to distinguish between the scenarios. Similar to many differentiated planetesimals that record isotope fractionation of non-traditional stable isotopic systems by evaporative processes for example, angrites (Si, Pringle et al., 2014), HED meteorites (K, Tian et al., 2019; Wang & Jacobsen, 2016), and lunar meteorites (K, Zn, Kato et al., 2015; Paniello, Moynier, et al., 2012), the ALC's PB has Zn isotopic signatures shifted toward heavier values, despite the fact that thermal evolution of the ALC PB ceased at an earlier stage.

Fe isotopic signatures of the ALC meteorites being slightly heavier than C-chondrites constitutes an unexpected find for PAs, which at first sight points toward a PB differentiation process, as if some parts of the PB that could represent a complimentary light reservoir were missing in the meteorite collections, for example, potential metal-enriched or basaltic reservoirs. However, the data presented here provide no support for Fe isotope fractionation by planetary differentiation processes. As an alternative hypothesis, the Fe isotopic signatures of ALC meteorites can result from a nebular process occurring before the PB accretion. However, a larger and more consistent data set of Fe isotope ratios, elemental compositions including values for the PGE, and O isotopic signatures is needed to confirm the nebular or PB origin of the Fe isotopic signatures of for ALC meteorites. Nevertheless, the Fe isotopic signatures of ALC meteoritic components record efficient thermal equilibration of metal and silicate reservoirs at the PB, as confirmed by the two-pyroxene thermometry. This suggests that the Fe isotope ratio data of ALC can be used in models of Fe isotopic differentiation during planetary processes, different to, for example, main group pallasites (Bennett et al., 2022; Chernonozhkin et al., 2016).

Acknowledgments—SCh acknowledges his postdoctoral fellowship from the Flemish Research Foundation (FWO) in the context of an "Excellence of Science (EoS)" project (ET-HoME—ID 30442502) and the grant support from the Montanuniversität Leoben. SG and PhC acknowledge the support from the FWO and the VUB Strategic Research. SG, PhC, and VD acknowledge funding from the EoS project "ET-Home"; and SG, PhC, GH, and VD from the Belgian Science Policy (Belspo). VD thanks the FRS-FNRS for present support. FWO is acknowledged for providing the funding for the acquisition of the MC-ICP-MS instrumentation (ZW15-02—G0H6216N). FV acknowledges the support from FWO under the form of the aforementioned EoS project and BOF-UGent. FV also acknowledges Teledyne CETAC Technologies for logistic and financial support. US Antarctic meteorite samples have been recovered by the Antarctic Search for Meteorites (ANSMET) program, which has been funded by the NSF and NASA, and characterized and curated by the Department of Mineral Sciences of the Smithsonian Institution and Astromaterials Curation Office at NASA Johnson Space Center. The collection of meteorites for the research was lent by the National History Museum London. Dr. Natasha Almeida is acknowledged for curating the meteorite collection of the NHM London and for preparing the sample sections for this work. Dr. Wencke Wegner is thanked for assistance with the EMPA at the Naturhistorisches Museum Wien. The authors appreciate the editorial handling of the manuscript by Dr. Marc Caffe and thoughtful comments by Dr. Jasmeet K Dhaliwal and one anonymous reviewer, which helped to improve the quality of the manuscript.

Conflict of Interest Statement—The authors declare no conflict of interest.

Data Availability Statement—The data that supports the findings of this study are available in the tabulated form in the manuscript. The raw unprocessed data is available upon request.

Editorial Handling—Dr. Marc W. Caffee

REFERENCES

Barrat, J.-A., Zanda, B., Moynier, F., Bollinger, C., Liorzou, C., and Bayon, G. 2012. Geochemistry of CI Chondrites: Major and Trace Elements, and Cu and Zn Isotopes. *Geochimica et Cosmochimica Acta* 83: 79–92.

Baxter, D. C., Rodushkin, I., Engström, E., and Malinovsky, D. 2006. Revised Exponential Model for Mass Bias Correction Using an Internal Standard for Isotope Abundance Ratio Measurements by Multi-Collector Inductively Coupled Plasma Mass Spectrometry. *Journal of Analytical Atomic Spectrometry* 21: 427–430.

Bennett, N. R., Sio, C. K., Schauble, E., Lesher, C. E., Wimpenny, J., and Shahar, A. 2022. Iron Isotope Evidence of an Impact Origin for Main-Group Pallasites. *Geochemical Perspectives Letters* 23: 6–10.

Bridgestock, L. J., Williams, H., Rehkämper, M., Larner, F., Giscard, M. D., Hammond, S., Coles, B., et al. 2014. Unlocking the Zinc Isotope Systematics of Iron Meteorites. *Earth and Planetary Science Letters* 400: 153–164.

Brugier, Y.-A., Barrat, J.-A., Gueguen, B., Agranier, A., Yamaguchi, A., and Bischoff, A. 2019. Zinc Isotopic Variations in Ureilites. *Geochimica et Cosmochimica Acta* 246: 450–460.

Chernonozhkin, S. M., Goderis, S., Costas-Rodríguez, M., Claeys, P., and Vanhaecke, F. 2016. Effect of Parent Body Evolution on Equilibrium and Kinetic Isotope Fractionation: A Combined Ni and Fe Isotope Study of Iron and Stony-Iron Meteorites. *Geochimica et Cosmochimica Acta* 186: 168–188.

Chernonozhkin, S. M., González de Vega, C., Artemieva, N., Soens, B., Belza, J., Bolea-Fernandez, E., van Ginneken, M., et al. 2021. Isotopic Evolution of Planetary Crusts by Hypervelocity Impacts Evidenced by Fe in Microtektites. *Nature Communications* 12: 5646.

Chernonozhkin, S. M., McKibbin, S. J., Goderis, S., Van Malderen, S. J. M., Claeys, P., and Vanhaecke, F. 2021. New Constraints on the Formation of Main Group Pallasites Derived from In Situ Trace Element Analysis and 2D Mapping of Olivine and Phosphate. *Chemical Geology* 562: 119996.

Chernonozhkin, S. M., Weyrauch, M., Goderis, S., Oeser, M., McKibbin, S. J., Horn, I., Hecht, L., Weyer, S., Claeys, P., and Vanhaecke, F. 2017. Thermal Equilibration of Iron Meteorite and Pallasite Parent Bodies Recorded at the Mineral Scale by Fe and Ni Isotope Systematics. *Geochimica et Cosmochimica Acta* 217: 95–111.

Collinet, M., and Grove, T. L. 2020. Formation of Primitive Achondrites by Partial Melting of Alkali-Undepleted Planetesimals in the Inner Solar System. *Geochimica et Cosmochimica Acta* 277: 358–376. https://doi.org/10.1016/j.gca.2020.03.004.

Craddock, P. R., and Dauphas, N. 2011. Iron Isotopic Compositions of Geological Reference Materials and Chondrites. *Geostandards and Geoanalytical Research* 35: 101–123. https://doi.org/10.1111/j.1751-908X.2010.00085.x.

Dauphas, N., and Pourmand, A. 2015. Thulium Anomalies and Rare Earth Element Patterns in Meteorites and Earth: Nebular Fractionation and the Nugget Effect. *Geochimica et Cosmochimica Acta* 163: 234–261. https://doi.org/10.1016/j.gca.2015.03.037.

Dauphas, N., Pourmand, A., and Teng, F. 2009. Routine Isotopic Analysis of Iron by HR-MC-ICPMS: How Precise and how Accurate? *Chemical Geology* 267: 175–184. https://doi.org/10.1016/j.chemgeo.2008.12.011.

Dauphas, N., Roskosz, M., Alp, E. E., Golden, D. C., Sio, C. K., Tissot, F. L. H., Hu, M. Y., Zhao, J., Gao, L., and Morris, R. V. 2012. A General Moment NRIXS Approach to the Determination of Equilibrium Fe Isotopic Fractionation Factors: Application to Goethite and Jarosite. *Geochimica et Cosmochimica Acta* 94: 254–275.

Dauphas, N., Roskosz, M., Alp, E. E., Neuville, D. R., Hu, M. Y., Sio, C. K., Tissot, F. L. H., et al. 2014. Magma Redox and Structural Controls on Iron Isotope Variations in Earth's Mantle and Crust. *Earth and Planetary Science Letters* 398: 127–140.

Dhaliwal, J. K., Day, J. M. D., Corder, C. A., Tait, K. T., Marti, K., Assayag, N., Cartigny, P., Rumble, D., and Taylor, L. A. 2017. Early Metal-Silicate Differentiation During Planetesimal Formation Revealed by Acapulcoite and Lodranite Meteorites. *Geochimica et Cosmochimica Acta* 216: 115–140.

Dhaliwal, J. K., Day, J. M. D., and Moynier, F. 2018. Volatile Element Loss During Planetary Magma Ocean Phases. *Icarus* 300: 249–260.

Elardo, S. M., Shahar, A., Mock, T. D., and Sio, C. K. 2019. The Effect of Core Composition on Iron Isotope Fractionation between Planetary Cores and Mantles. *Earth and Planetary Science Letters* 513: 124–134.

Fischer-Gödde, M., Becker, H., and Wombacher, F. 2010. Rhodium, Gold and Other Highly Siderophile Element Abundances in Chondritic Meteorites. *Geochimica et Cosmochimica Acta* 74: 356–379.

Floss, C. 2000. Complexities on the Acapulcoite-Lodranite Parent Body: Evidence from Trace Element Distributions in Silicate Minerals. *Meteoritics & Planetary Science* 35: 1073–85.

Galy, A., Yoffe, O., Janney, P. E., Williams, R. W., Cloquet, C., Alard, O., et al. 2003. Magnesium Isotope Heterogeneity of the Isotopic Standard SRM980 and New Reference Materials for Magnesium-Isotope-Ratio Measurements. *Journal of Analytical Atomic Spectrometry* 18: 1352.

González de Vega, C., Chernonozhkin, S. M., Grigoryan, R., Costas-Rodríguez, M., and Vanhaecke, F. 2020. Characterization of the New Isotopic Reference Materials IRMM-524A and ERM-AE143 for Fe and Mg Isotopic Analysis of Geological and Biological Samples. *Journal of Analytical Atomic Spectrometry* 35: 2517–29.

Goodrich, C. A., and Delaney, J. S. 2000. Fe/Mg-Fe/Mn Relations of Meteorites and Primary Heterogeneity of Primitive Achondrite Parent Bodies. *Geochimica et Cosmochimica Acta* 64: 149–160.

Greenwood, R. C., Burbine, T. H., Miller, M. F., and Franchi, I. A. 2017. Melting and Differentiation of Early-Formed Asteroids: The Perspective from High Precision Oxygen Isotope Studies. *Geochemistry* 77: 1–43.

Grigoryan, R., Costas-Rodríguez, M., Vandenbroucke, R. E., and Vanhaecke, F. 2020. High-Precision Isotopic Analysis of Mg and Ca in Biological Samples Using Multi-Collector ICP-Mass Spectrometry after their Sequential Chromatographic Isolation – Application to the Characterization of the Body Distribution of Mg and Ca Isotopes in Mice. *Analytica Chimica Acta* 1130: 137–145.

Hezel, D. C., Needham, A. W., Armytage, R., Georg, B., Abel, R. L., Kurahashi, E., Coles, B. J., Rehkämper, M., and Russell, S. S. 2010. A Nebula Setting as the Origin for Bulk Chondrule Fe Isotope Variations in CV Chondrites. *Earth and Planetary Science Letters* 296: 423–433.

Huang, F., Chen, L., Wu, Z., and Wang, W. 2013. First-Principles Calculations of Equilibrium Mg Isotope Fractionations Between Garnet, Clinopyroxene, Orthopyroxene, and Olivine: Implications for Mg Isotope Thermometry. *Earth and Planetary Science Letters* 367: 61–70.

Jochum, K. P., Nohl, U., Herwig, K., Lammel, E., Stoll, B., and Hofmann, A. W. 2005. GeoReM: A New Geochemical Database for Reference Materials and Isotopic Standards. *Geostandards and Geoanalytical Research* 29: 333–38.

Johnson, C. M., Beard, B. L., and Weyer, S. 2020. High-Temperature Fe Isotope Geochemistry. In *Iron Geochemistry: An Isotopic Perspective*, 85–147. Cham: Springer.

Kallemeyn, G. W., Rubin, A. E., Wang, D., and Wasson, J. T. 1989. Ordinary Chondrites: Bulk Compositions, Classification, Lithophile-Element Fractionations and Composition-Petrographic Type Relationships. *Geochimica et Cosmochimica Acta* 53: 2747–67.

Kato, C., Moynier, F., Valdes, M. C., Dhaliwal, J. K., and Day, J. M. D. 2015. Extensive Volatile Loss During Formation and Differentiation of the Moon. *Nature Communications* 6: 7617.

Keil, K., and McCoy, T. J. 2018. Acapulcoite-lodranite Meteorites: Ultramafic Asteroidal Partial Melt Residues. *Chemie der Erde* 78: 153–203.

Krot, A. N., Keil, K., Scott, E. R. D., Goodrich, C. A., and Weisberg, M. K. 2014. Classification of Meteorites and their Genetic Relationships. In *Treatise on Geochemistry*. *Volume 1: Meteorites, Comets, and Planets*, 2nd ed., 1–63. Amsterdam, Netherlands: Elsevier.

Larsen, K. K., Schiller, M., and Bizzarro, M. 2016. Accretion Timescales and Style of Asteroidal Differentiation in an ^{26}Al-Poor Protoplanetary Disk. *Geochimica et Cosmochimica Acta* 176: 295–315.

Li, S., Yin, Q. Z., Bao, H., Sanborn, M. E., Irving, A., Ziegler, K., Agee, C., et al. 2018. Evidence for a Multilayered Internal Structure of the Chondritic Acapulcoite-Lodranite Parent Asteroid. *Geochimica et Cosmochimica Acta* 242: 82–101.

Lodders, K. 2003. Solar System Abundances and Condensation Temperatures of the Elements. *The Astrophysical Journal* 591: 1220–47.

Lucas, M. P., Dygert, N., Ren, J., Hesse, M. A., Miller, N. R., and McSween, H. Y. 2022. Thermochemical Evolution of the Acapulcoite–Lodranite Parent Body: Evidence for Fragmentation-Disrupted Partial Differentiation. *Meteoritics & Planetary Science* 57: 2248–75.

Lucas, M. P., Emery, J. P., Hiroi, T., and McSween, H. Y. 2019. Spectral Properties and Mineral Compositions of Acapulcoite-Lodranite Clan Meteorites: Establishing S-Type Asteroid-Meteorite Connections. *Meteoritics & Planetary Science* 54: 157–180.

Luck, J.-M., Othman, D. B., and Albarède, F. 2005. Zn and Cu Isotopic Variations in Chondrites and Iron Meteorites: Early Solar Nebula Reservoirs and Parent-Body Processes. *Geochimica et Cosmochimica Acta* 69: 5351–63.

Maréchal, C. N., Télouk, P., and Albarède, F. 1999. Precise Analysis of Copper and Zinc Isotopic Compositions by Plasma-Source Mass Spectrometry. *Chemical Geology* 156: 251–273.

McCoy, T. J., Keil, K., Muenow, D. W., and Wilson, L. 1997. Partial Melting and Melt Migration in the Acapulcoite-Lodranite Parent Body. *Geochimica et Cosmochimica Acta* 61: 639–650.

McCoy, T. J., Keil, K., Clayton, R. N., Mayeda, T. K., Bogard, D. D., Garrison, D. H., Huss,G. R., Hutcheon, I. D., & Wieler, R. (1996). A petrologic, chemical, and isotopic study of Monument Draw and comparison with other acapulcoites: Evidence for formation by incipient partial melting. *Geochimica et Cosmochimica Acta*, 60(14), 2681–2708.

Mittlefehldt, D. W. 2014. Achondrites. In *Treatise on Geochemistry*. *Volume 1: Meteorites, Comets, and Planets*, 2nd ed., 235–266. Amsterdam, Netherlands: Elsevier.

Morikawa, N., and Nakamura, N. 1997. Silicate Melt Migration in the Acapulcoite-Lodranite Source Inferred from Alkali and Rare-Earth-Element Abundances. *Meteoritics & Planetary Science* 32, A94.

Moynier, F., Beck, P., Yin, Q.-Z., Ferroir, T., Barrat, J.-A., Paniello, R. C., Telouk, P., and Gillet, P. 2010. Volatilization Induced by Impacts Recorded in Zn Isotope Composition of Ureilites. *Chemical Geology* 276: 374–79.

Moynier, F., Paniello, R. C., Gounelle, M., Albarède, F., Beck, P., Podosek, F., and Zanda, B. 2011. Nature of Volatile Depletion and Genetic Relationships in Enstatite Chondrites and Aubrites Inferred from Zn Isotopes. *Geochimica et Cosmochimica Acta* 75: 297–307.

Nakamuta, Y., Urata, K., Shibata, Y., and Kuwahara, Y. 2017. Effect of NaCrSi2O6 Component on Lindsley's Pyroxene Thermometer: An Evaluation Based on Strongly Metamorphosed LL Chondrites. *Meteoritics & Planetary Science* 52: 511–521.

Needham, A. W., Porcelli, D., and Russell, S. S. 2009. An Fe Isotope Study of Ordinary Chondrites. *Geochimica et Cosmochimica Acta* 73: 7399–7413.

Neumann, W., Henke, S., Breuer, D., Gail, H.-P., Schwarz, W. H., Trieloff, M., Hopp, J., and Spohn, T. 2018. Modeling the Evolution of the Parent Body of Acapulcoites and Lodranites: A Case Study for Partially Differentiated Asteroids. *Icarus* 311: 146–169.

Paniello, R. C., Day, J. M. D., and Moynier, F. 2012. Zinc Isotopic Evidence for the Origin of the Moon. *Nature* 490: 376–79.

Paniello, R. C., Moynier, F., Beck, P., Barrat, J.-A., Podosek, F. A., and Pichat, S. 2012. Zinc Isotopes in HEDs: Clues to the Formation of 4-Vesta, and the Unique Composition of Pecora Escarpment 82,502. *Geochimica et Cosmochimica Acta* 86: 76–87.

Pettke, T., Oberli, F., Audétat, A., Guillong, M., Simon, A. C., Hanley, J. J., and Klemm, L. M. 2012. Recent Developments in Element Concentration and Isotope Ratio Analysis of Individual Fluid Inclusions by Laser Ablation Single and Multiple Collector ICP-MS. *Ore Geology Reviews* 44: 10–38.

Poitrasson, F. 2007. Does Planetary Differentiation Really Fractionate Iron Isotopes? *Earth and Planetary Science Letters* 256: 484–492.
Poitrasson, F., Levasseur, S., and Teutsch, N. 2005. Significance of Iron Isotope Mineral Fractionation in Pallasites and Iron Meteorites for the Core–Mantle Differentiation of Terrestrial Planets. *Earth and Planetary Science Letters* 234: 151–164.
Pringle, E. A., Moynier, F., Beck, P., Paniello, R. C., and Hezel, D. C. 2017. The Origin of Volatile Element Depletion in Early Solar System Material: Clues from Zn Isotopes in Chondrules. *Earth and Planetary Science Letters* 468: 62–71.
Pringle, E. A., Moynier, F., Savage, P. S., Badro, J., and Barrat, J.-A. 2014. Silicon Isotopes in Angrites and Volatile Loss in Planetesimals. *Proceedings of the National Academy of Sciences of the United States of America* 111: 17029–32.
Putirka, K. D. 2008. Thermometers and Barometers for Volcanic Systems. *Reviews in Mineralogy and Geochemistry* 69: 61–120.
Render, J., Brennecka, G. A., Burkhardt, C., and Kleine, T. 2022. Solar System Evolution and Terrestrial Planet Accretion Determined by Zr Isotopic Signatures of Meteorites. *Earth and Planetary Science Letters* 595: 117748. https://doi.org/10.1016/j.epsl.2022.117748.
Rüfenacht, M., Morino, P., Lai, Y.-J., Fehr, M. A., Haba, M. K., and Schönbächler, M. 2023. Genetic Relationships of Solar System Bodies Based on their Nucleosynthetic Ti Isotope Compositions and Sub-Structures of the Solar Protoplanetary Disk. *Geochimica et Cosmochimica Acta* 355: 110–125.
Schiller, M., Dallas, J. A., Creech, J. B., Bizzarro, M., and Baker, J. A. 2017. Tracking the Formation of Magma Oceans in the Solar System Using Stable Magnesium Isotopes. *Geochemical Perspectives Letters* 3: 22–31.
Schoenberg, R., and Von Blanckenburg, F. 2006. Modes of Planetary-Scale Fe Isotope Fractionation. *Earth and Planetary Science Letters* 252: 342–359.
Sedaghatpour, F., and Teng, F.-Z. 2016. Magnesium Isotopic Composition of Achondrites. *Geochimica et Cosmochimica Acta* 174: 167–179. https://doi.org/10.1016/j.gca.2015.11.016.
Soens, B., van Ginneken, M., Chernonozhkin, S. M., Slotte, N., Debaille, V., Vanhaecke, F., Terryn, H., Claeys, P., and Goderis, S. 2021. Australasian Microtektites across the Antarctic Continent: Evidence from the Sør Rondane Mountain Range (East Antarctica). *Geoscience Frontiers* 12: 101153.
Sossi, P. A., Nebel, O., Anand, M., and Poitrasson, F. 2016. On the Iron Isotope Composition of Mars and Volatile Depletion in the Terrestrial Planets. *Earth and Planetary Science Letters* 449: 360–371.
Teng, F.-Z., Dauphas, N., and Helz, R. T. 2008. Iron Isotope Fractionation during Magmatic Differentiation in Kilauea Iki Lava Lake. *Science* 320: 1620–22.
Teng, F.-Z., Dauphas, N., and Watkins, J. M. 2017. Non-Traditional Stable Isotopes: Retrospective and Prospective. *Reviews in Mineralogy and Geochemistry* 82: 1–26.
Teng, F.-Z., Li, W.-Y., Ke, S., Marty, B., Dauphas, N., Huang, S., Wu, F.-Y., and Pourmand, A. 2010. Magnesium Isotopic Composition of the Earth and Chondrites. *Geochimica et Cosmochimica Acta* 74: 4150–66.
Tian, Z., Chen, H., Fegley, B., Lodders, K., Barrat, J.-A., Day, J. M. D., and Wang, K. 2019. Potassium Isotopic Compositions of Howardite-Eucrite-Diogenite Meteorites. *Geochimica et Cosmochimica Acta* 266: 611–632.
Touboul, M., Kleine, T., Bourdon, B., Van Orman, J. A., Maden, C., and Zipfel, J. 2009. Hf–W Thermochronometry: II. Accretion and Thermal History of the Acapulcoite–Lodranite Parent Body. *Earth and Planetary Science Letters* 284: 168–178. https://doi.org/10.1016/j.epsl.2009.04.022.
Van Heghe, L., Engström, E., Rodushkin, I., Cloquet, C., and Vanhaecke, F. 2012. Isotopic Analysis of the Metabolically Relevant Transition Metals Cu, Fe and Zn in Human Blood from Vegetarians and Omnivores Using Multi-Collector ICP-Mass Spectrometry. *Journal of Analytical Atomic Spectrometry* 27: 1327.
Wang, K., and Jacobsen, S. B. 2016. Potassium Isotopic Evidence for a High-Energy Giant Impact Origin of the Moon. *Nature* 538: 487–490.
Wang, K., Moynier, F., Barrat, J., Zanda, B., Paniello, R. C., and Savage, P. S. 2013. Homogeneous Distribution of Fe Isotopes in the Early Solar Nebula. *Meteoritics & Planetary Science* 48: 354–364.
Wang, K., Savage, P. S., and Moynier, F. 2014. The Iron Isotope Composition of Enstatite Meteorites: Implications for their Origin and the Metal/Sulfide Fe Isotopic Fractionation Factor. *Geochimica et Cosmochimica Acta* 142: 149–165.
Wasson, J. T., and Kallemeyn, G. W. 1988. Compositions of Chondrites. *Philosophical Transactions of the Royal Society A: Mathematical, Physical and Engineering Sciences* 325: 535–544.
Weyer, S., Anbar, A. D., Brey, G. P., Munker, C., Mezger, K., Woodland, A. B., Münker, C., Mezger, K., and Woodland, A. B. 2005. Iron Isotope Fractionation During Planetary Differentiation. *Earth and Planetary Science Letters* 240: 251–264.
Wombacher, F., Eisenhauer, A., Heuser, A., and Weyer, S. 2009. Separation of Mg, Ca and Fe from Geological Reference Materials for Stable Isotope Ratio Analyses by MC-ICP-MS and Double-Spike TIMS. *Journal of Analytical Atomic Spectrometry* 24: 627.
Young, E. D., and Scott, E. R. D. 2021. Revisiting the Wasson Fractional Crystallization Model for IIIAB Iron Meteorites with Implications for the Interpretation of their Fe Isotope Ratios. *Meteoritics & Planetary Science* 57: 228–237. https://doi.org/10.1111/maps.13752.
Zhu, X. K., Guo, Y., O'Nions, R. K., Young, E. D., and Ash, R. D. 2001. Isotopic Homogeneity of Iron in the Early Solar Nebula. *Nature* 412: 311–13.

SUPPORTING INFORMATION

Additional supporting information may be found in the online version of this article.

Figure S1. 2D μXRF maps showing the distribution of Fe and Si in a 1-inch section of Dhofar 125 acapulcoite.

Figure S2. Plots of $\delta^{26/24}$Mg results for ALC meteorites.

Figure S3. Scatter plots of CI chondrite normalized mass fractions of Sm versus Dy in augite of ALC meteorites.

Figure S4. Plots of $\delta^{56/54}$Fe, $\delta^{26/24}$Mg and $\delta^{66/64}$Zn values for whole rock ALC meteorites versus chondrite-normalised mass fractions of Sm in augite.

Figure S5. Plots of $\delta^{56/54}$Fe, $\delta^{26/24}$Mg and $\delta^{66/64}$Zn values for whole rock ALC meteorites versus the molar ratio of Fe/Mn in augite.

Figure S6. Plots of $\delta^{56/54}$Fe, $\delta^{26/24}$Mg, and $\delta^{66/64}$Zn results for acapulcoite lodranite meteorites versus their oxygen isotopic composition (Greenwood et al., 2017).

Figure S7. SEM-BSE images of LAR 06605 lodranite (a) and EET 84302 transitional acapulcoite/lodranite (b). The oxidized metal areas are highlighted in yellow.

Figure S8. Plots of $\delta^{56/54}$Fe versus $\delta^{57/54}$Fe, $\delta^{26/24}$Mg versus $\delta^{25/24}$Mg, and $\delta^{66/64}$Zn versus $\delta^{68/64}$Zn results for the characterized acapulcoite lodranite meteorites, demonstrating the mass-dependent nature of the measured signatures.

Figure S9. The box and whiskers plot for (a) $\delta^{56/54}$Fe and (b) $\delta^{26/24}$Mg values of the whole rock ALC (this work) and C-chondrites, ordinary chondrites, and enstatite chondrites.